states, which means that a HOMO-LUMO light excitation would not modify the spin population of the substrate. In the perspective of producing a spin excitation through these HOMO-LUMO light excitations, the only possibility is to modify the spin population of the molecular Fe atom and through the super-exchange coupling with the Ni underneath to have some effect on the latter. The modifications on the Fe atom are, however, too light to have a significant effect on the Ni underneath. Other transitions could be considered at higher energies. However, these involve states of higher mixing between the molecule and substrate orbitals, making a plausible tuning more complex.

CHAPTER 9

Magnonic studies

Built the Heisenberg Hamiltonian of a magnetic system, its diagonalization gives the system spin coherent excitations, which are called magnons (see Section 2.3.2).

The interest in this chapter is to obtain an Heisenberg Hamiltonian of the FePc/NiO(001) spinterface and to evaluate the effect of the molecule adsorption on the substrate magnonic properties. In this regard, effects of the adsorption of organic compounds on the inorganic substrate magnonic properties have already been observed, e.g. the experimental results on YIG [5] and the theoretical ones on CrSBr [78, 79]. The magnonic group velocity is affected by the charge transfer mechanisms at the interface. Still these kind of studies are missing for TM-oxides layers, in spite of their remarkable characteristics in terms of magnonics: low spin-orbit coupling, antiferromagnetic and insulating character.

9.1 Computational details

With respect to the computational details of the preceding Chapter 8 there are some differences and some additions. The value considered for the Ni atoms $U_{Ni} = 5.8$ eV is chosen in order to properly reproduce the expected experimental values of the NiO bulk magnonic bands [157]-[158], while the one chosen for the Fe atom is unchanged. In this regard, we have verified that choosing a different U for the Fe atom changes only the local super-exchange coupling Fe-O-Ni, not having any significant effect on the average values of the substrate. This means that if we are interested in the average effects on the substrate, the U value of the Fe atom is not as significant as the one of the Ni atoms. The selected plane wave cutoff is here 70 Ry for the wavefunctions. The minimal adsorption energy configuration is the one underlined in the literature [119] and reported in the preceding chapter 8, properly optimized with the new parameters.

Additional computational methods are here described. In particular, a wannierisation procedure allows us to extract from the DFT results a tight-binding model of the system. This is then used in a perturbative approach based on magnetic force theorem (MFT), to extract the exchange couplings of an Heisenberg model:

$$\hat{H} = \frac{1}{2} \sum_{i,j} J_{i,j} \hat{S}_i \hat{S}_j \tag{9.1}$$

where only collinear terms have been considered. A downfolding is applied in the extraction of the exchange couplings, due to the presence of the O ligands in the substrate. At this point, a Holstein-Primakoff transformation of the spin operator in the Heisenberg model allows us to introduce annihilation/creation operators of quasiparticle quanta, i.e. magnons, and to extract from the Heisenberg model their dispersion law through a diagonalization procedure (Colpa's method) [111].

9.2 NiO bulk

The NiO in its rock-salt structure with a lattice parameter of 4.168 Å is considered in its antiferromagnetic ordering AFII (stacking of ferromagnetic planes along the [111] direction) [156]. Between the exchange couplings the non-null ones are the J1 and J2 couplings, respectively, along the ferromagnetic planes $[111]$ and between the ferromagnetic planes $[111]$ not through the O atoms, and the J3 couplings between the ferromagnetic planes $[111]$ but this time through the O atoms. The J3 coupling is the most significant one and it is due to super-exchange coupling [159]. These couplings are indicated in the Fig. 9.1 by the colored lines.

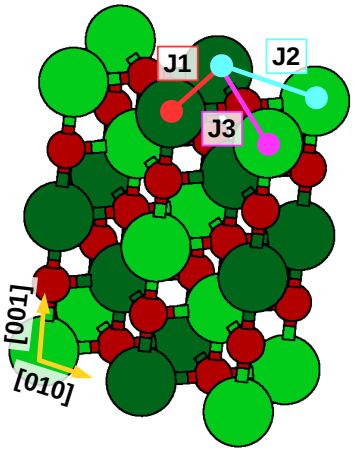

Figure 9.1 NiO bulk conventional unit cell of 8 formula units (FU). Color scheme as follows. Light (up) and dark (down) green: Ni atoms, according to their magnetization; Red: O. The main exchange couplings between the Ni atoms are indicated through a colored line: Red: J1; Ciano: J2; and Magenta: J3.

Different effective U values have been considered in the calculation of the exchange couplings, Fig. 9.3. As highlighted in the computational details, first a wannierisation procedure is considered to extract a tight-binding Hamiltonian, then the MFT is applied to the tight-binding Hamiltonian to extract the exchange couplings.

In the wannierisation procedure a projection approach has been used, considering as initial projectors p orbitals for the O and d orbitals for the Ni, in an energy window $[-12, a)$ eV around the Fermi energy, where a has been modified in order to include the d orbitals bands at the bottom of the conduction band for varying U value. This choice for the energy window is clarified by looking at the band structure in Fig. 9.2 at a fixed U value, where a colored circle represents the contribution to the respective Kohn-Sham state of the pointed atomic orbital. No localization iteration has been applied in the wannierisation, in order to avoid spurious hybridisations between the p orbitals and the d orbitals in the building of the tight-binding Hamiltonian.

Then from the tight-binding Hamiltonian, trough the MFT we have obtained the isotropic exchange couplings.

The noise introduced by the wannierisation procedure has been evaluated through a fitting of the tight-binding Hamiltonian energy bands and the DFT energy bands. This fitting allows us to estimate qualitatively an error on the J values as $E_W \sim [\eta/(W/N_b)] * [\eta_{\max}/t_{\max}]$ where W is the energy window opening, N_b the number of wannierised bands, $t_{\max}(\ 2eV)$ the maximum band width in the energy window, and η the average

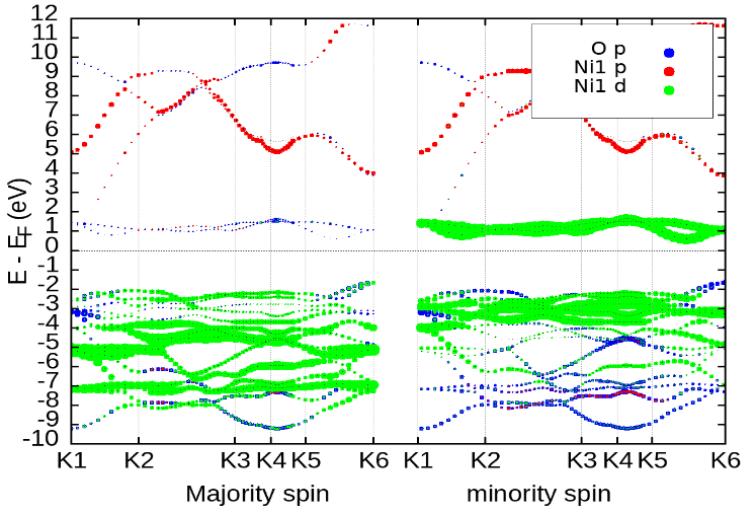

Figure 9.2 Electronic fat-bands structure of NiO bulk (U=4.00 eV). Color scheme as follows: Blue: O p orbitals; Red: Ni1 p orbitals; Green: Ni1 d orbitals; where Ni1 is the Ni majority spin channel species in the AF phase. Majority spin channel components are shown on the right, while minority spin channel component on the left. The position of the Fermi energy in the gap is arbitrary.

noise on the wannierisation

$$\eta = \sqrt{\frac{1}{N_k}\sum_{mk}(E_{\text{DFT},mk} - E_{\text{WAN},mk})^2} \tag{9.2}$$

with the maximum deviation measured as $\eta_{\text{max}} = \max_{mk}|E_{\text{DFT},mk} - E_{\text{WAN},mk}|$.

As can be observed, the noise for U parameters outside the intervall [4.5,6.5] is quite significant ($> 20\%$), as the wannierisation becomes more difficult; to relax the structure with the corresponding U can help into obtaining a better wannierisation; however, here, we have fixed the lattice parameter in order to reproduce the experimental one.

From the ground state point of view, here we remind that, to an increase in U corresponds an increase in the magnetic moment on the Ni, and a respective decrease in charge on the Ni and increase in charge on the O. Thus, looking at Fig. 9.3, we can conclude that an increase of magnetic moment on the Ni (and increase in electronic charge) corresponds to a decrease in absolute value of the associated J3 coupling.

We selected an effective U of 5.8 eV for the Ni atoms, which gives exchange couplings in between the experimental results [157, 158]: $J1 = 0.41$, $J2 = -0.17$ and $J3 = -9.02$ meV, as well as the lowest noise in the chosen wannierisation procedure as underlined by the minimum of E_W in Fig. 9.3 and by the close overlap of the bands in Fig. 9.4.

9.3 FePc/NiO(001)

From the NiO(001) 1×1 cell we have built a supercell, considering an epitaxy matrix $((6,0)(3,3))$, as in the preceding chapter. After a first relaxation of the surface, we have

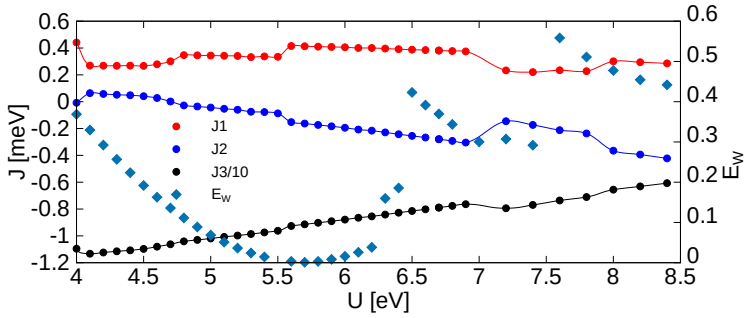

Figure 9.3 Main exchange couplings in the NiO bulk for different U values: J1 (Red) and J2 (Dark-Blue) between Ni atoms along the [111] planes, and J3 (Black) between different [111] planes, through the O atoms. It is reported a qualitative evaluation of the error on the Js due to the Wannierisation procedure (Light-Blue).

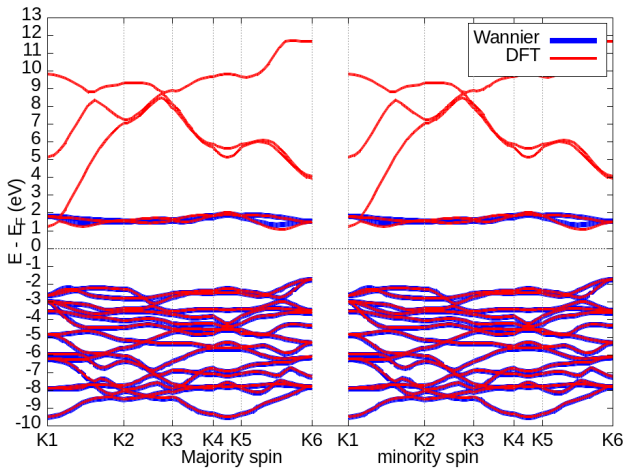

Figure 9.4 Electronic band structure of NiO bulk (U=5.80 eV). Solid/dash-dotted lines indicate DFT and Wannier results, respectively. Spin-up components are shown on the right, while spin-down on the left. The position of the Fermi energy in the gap is arbitrary.

positioned the molecule in its minimum adsorption configuration, as reported in Chapter 8. The different U parameter of the substrate from the preceding chapter makes the molecule to get closer to the substrate, changing its electronic structure. This highlights then a different minimum adsorption configuration from the one of the preceding chapter. Since the differences are mainly in the molecular part of the spinterface, and being in this chapter interested in the substrate part, we have preferred an accurate description of the former even at the expense of the latter. The Fe atom moves toward the surface, thereby bonding more closely with the O below (Fe-O 2.05 Å), which moves upwards by 0.10 ± 0.03 Å of the surface. The rest of the molecule is left behind 2.9 ± 0.1 Å and not dragged by the Fe atom. The Fe changes its d orbital filling and undergoes a spin-crossover transition: $d^{\downarrow}_{z^2} d^{\uparrow\downarrow}_{xz} d^{\downarrow}_{yz} d^{\uparrow\downarrow}_{xy}$ to $d^{\downarrow}_{z^2} d^{\downarrow}_{xz} d^{\downarrow}_{yz} d^{\downarrow}_{xy} d^{\uparrow\downarrow}_{x^2-y^2}$ with consequent effect on its

magnetic moment $-2.17\mu_B \rightarrow -3.76\mu_B$. The magnetic variations on the substrate are analogous, apart differences in the order of $1 \times 10^{-3}\mu_B$, with the ones already reported. The charge transfer from the molecule toward the surface is now of 0.35 electrons, with respect to the 0.25 of the preceding chapter.

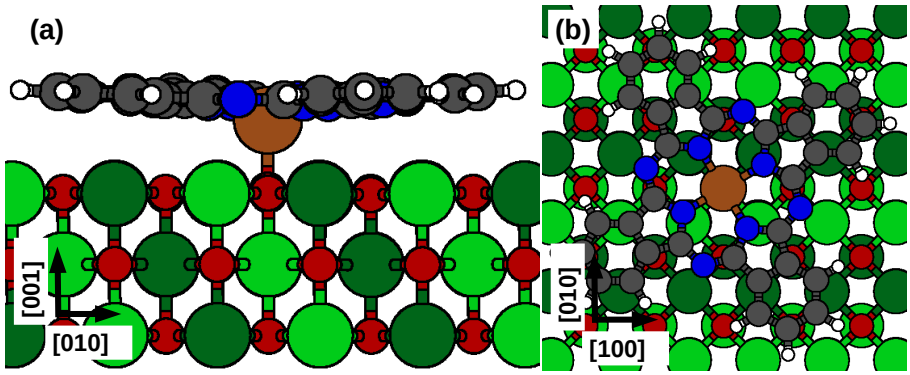

Figure 9.5 Side-view (a) and top-view (b) of the minimum adsorption energy configuration of FePc/NiO(001). Color scheme as follows. Light (up) and dark (down) green: Ni atoms, according to their magnetization; Red: O; Brown: Fe; Blue: N; Dark-gray: C; Light-gray: H.

A projection approach has been used in the wannierisation procedure, considering as initial projectors p orbitals for the O, C, N and d orbitals for the Ni and Fe, in an energy window $[-9, 1)$ eV around the Fermi energy. No localization iteration has been applied, in order to avoid spurious hybridisation between the different orbitals in the building of the tight-binding Hamiltonian.

Due to the fact that a single $\boldsymbol{k}$ point (Γ) has been considered in the calculations, the quality of the wannierisation has been evaluated looking at the PDOS (Fig. 9.6), instead of the band structure as in the bulk calculations (the PDOS here calculated is similar to the one of the preciding chapter). The error on the J values is, then, qualitatively associated to a different definition of the average noise on the wannierisation ($\sim \eta * \eta_{max}$):

$$\eta = \sqrt{\sum_i \left(\frac{w_{DFT,i} - w_{Wan,i}}{w_{DFT,i} + w_{Wan,i}} \right)^2} \tag{9.3}$$

where $w_i = | < \psi_i | A > |^2$ is the projection of the Kohn-Sham states in the energy bin i (having a width of 0.1 eV) over the atomic orbitals of the atom A (the different atomic groups have been considered: C atoms, N atoms, molecule and substrate). Note that the maximum absolute value of the deviation between the different bins is measured by η_{max}. For the clean substrate the error is of 0.04, while for the adsorbed system the error is of 0.07.

Following the wannierisation, we have extracted the exchange couplings for the clean substrate and for the adsorbed one, and compared the two (Fig. 9.7).

We have attempted to understand how the variations in the exchange couplings ΔJ due to the molecule adsorption correlate to other electronic/magnetic variations, calculating their rank correlation (Spearman's correlation [160, 161]), in order to asses any

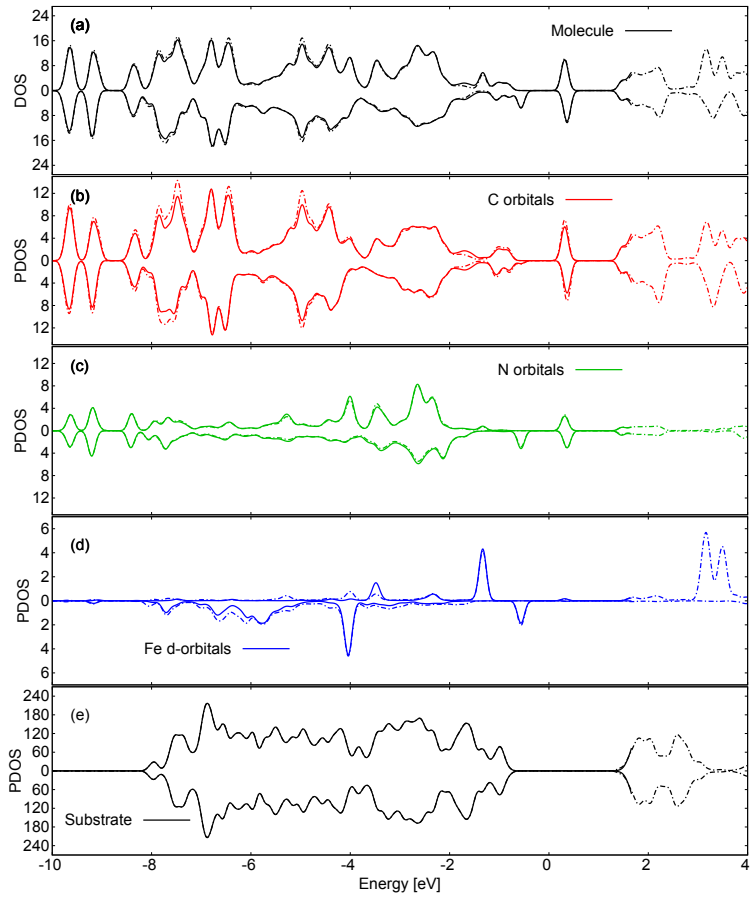

Figure 9.6 Electronic PDOS of FePc/NiO(001) summed over (a) all molecule atoms; (b) C; (c) N; (d) Fe; (e) substrate atoms. Solid/dash-dotted lines indicate Wannier and DFT results, respectively. Spin-down components are shown as negative values. All values in states/eV/cell. The position of the Fermi energy in the gap is arbitrary.

monotonic relationship between the variations:

$$r_s = \frac{cov(R(X), R(Y))}{\sigma_{R(X)}\sigma_{R(Y)}} \tag{9.4}$$

where the rank of a variable $R(X)$ is its ordinal value (i.e. from $X = \{0.5, 1.3, 0.01\}$ follows $R(X) = \{2, 3, 1\}$), σ is the standard deviation, and cov the covariance. From here, it emerges how the local variations in the super-exchange couplings $J3$ in the top layer are weakly correlated to local variations in the electronic densities of the O atoms ($\simeq 0.40$ with a p-value of < 0.01) (Pearson's correlation gives analogue results, but slightly smaller correlations, i.e. $\simeq 18\%$), while it is not clear if there is any correlation with the redistribution of charge in the p-orbitals of the O atoms ($\simeq -0.14$ with a p-value of 0.20),

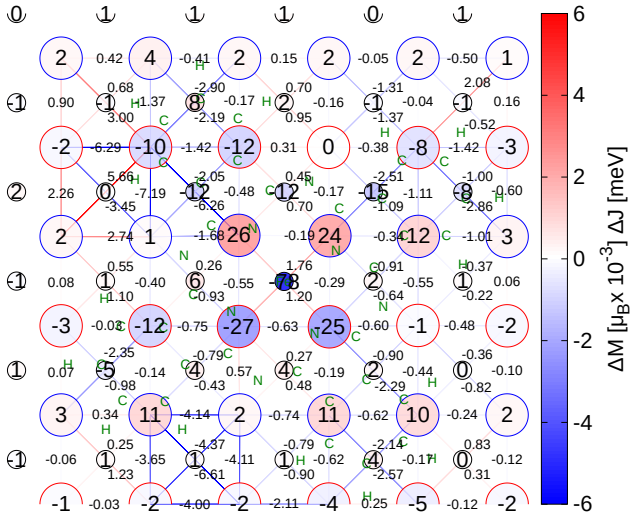

Figure 9.7 Changes in the exchange couplings and in the atomic magnetic moments of the substrate of FePc/NiO(0001) with respect to the pristine substrate (positive=increase in the quantity). The position of the molecule atoms is marked by green letters. The circles represent the atoms, the small ones the O atoms, while the big ones the Ni atoms; the filling color of each circle is the corresponding variation in the magnetic moment ΔM (the number in the circle quantifies this variation), the color of the contour of each Ni circle represents its initial magnetization before the molecule adsorption. The colored lines between pair of atoms represent the variations in the exchange couplings between the pair ΔJ (the little number on the line quantifies this variation).

where the latter has been described through the coefficient

$$Deff_i = \frac{||p_i - p_i^0||_2}{||p_i^0||_2} \tag{9.5}$$

where $p_i = (p_i^x, p_i^y, p_i^z)$ is the electron charge of the p orbital of the O atom i, and $||\cdot||_2$ the usual 2-norm. Associating to each J3 coupling, instead, the average of the magnetic moment variations of the two bonding Ni atoms, while in general does not seem to be any correlation ($\simeq 0.06$ with a p-value of 0.32), taking into account only the J3 couplings between the top and the bottom layers, it emerges a weak correlation ($\simeq -0.23$ with a p-value of 0.18). These correlations highlight two effects in the variations of the super-exchange couplings: the depletion of electronic charge in the O atoms is correlated to an increase of the super-exchange couplings, while the decrease of the Ni magnetic moments is correlated to a decrease of the super-exchange couplings. It is important to note here, it is the fact that the reduction of the Ni magnetic moment is due to the filling of the half-empty e_g states. Moreover, the filling charge is not the one from the molecule, but mainly the one leaving the O at the surface; this mechanism appears as well in the other substrates, as the Cr_2O_3(0001) O-terminated one and CoO(001) one (in some way,

the molecule reduces the local correlation of the TM ions at the surface, favoring the electron migration).

An average of the exchange couplings can support these two main effects better than our correlation results. In Table 9.1, the effects underlined above are shown by J3 top and by J3 top-bottom. Moreover, it is clear how the molecule is mainly affecting the atoms nearby, as no variations can be observed in the middle and bottom layers. We expect that increasing the number of layers, the J3 between different layers would converge towards a bulk-like value.

Table 9.1 Comparison between the exchange couplings of the supercell with and without the molecule: the results are down-folded (symmetrized) into the unitary cell. The differentiation between J1,J2 and J3 is analogue to the one of the bulk. The slab nature is properly considered differentiating between the different layers (intra-layers and inter-layers).

		Substrate	**Substrate+Molecule [meV]**
Intra-layers			
Top	J1	0.52	-0.48
	J2	0.14	-0.48
	J3	-7.81	-8.48
Middle	J1	0.07	0.25
	J2	-0.22	-0.29
	J3	-10.18	-10.19
Bottom	J1	0.52	0.65
	J2	0.14	0.03
	J3	-7.81	-7.71
Inter-layers			
Top-Middle	J1	-0.36	-0.18
	J2	-1.14	-0.57
Bottom-Middle	J1	-0.37	-0.18
	J2	-1.14	-0.57
Top-Bottom	J3	-16.72	-13.52

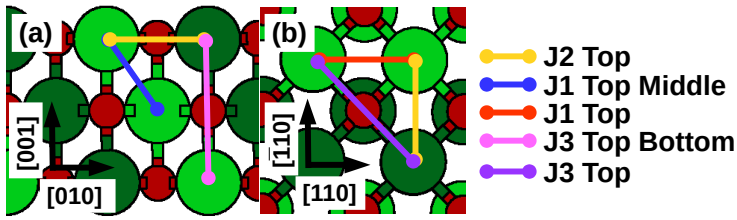

Figure 9.8 Side-view (a) and top-view (b) of the substrate NiO(001). The exchange-couplings are underlined through colored lines: Yellow: J2 in the Top layer; Pink: J3 between Top-Bottom layers; Blue: J1 between Top-Middle layers; Purple: J3 in the Top layer; Orange: J1 in the Top layer. The other exchange-couplings are easily identified. The color scheme of the atoms is as the one of the above figure.

From this table we can obtain the magnonic dispersion of the clean substrate and of the adsorbed substrate as shown in Fig. 9.9. In details, first an Heisenberg model of the NiO(001)1x1 (3 layers) cell is built, considering these values as the exchange values between the atoms of the cell, then this Heisenberg model is diagonalized as specified in Section 2.3.2.

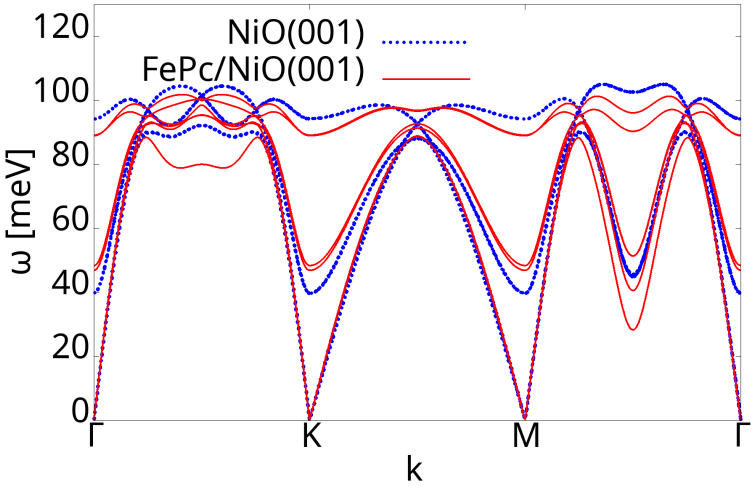

Figure 9.9 Magnonic bands of the pristine substrate (Blue) and adsorbed substrate (Red). These have been obtained through Linear Spin Wave theory, considering only the quadratic collinear terms in the Heisenberg Hamiltonian.

Looking at the magnonic dispersion, we can observe as overall the reduction of the exchange couplings has a small effect. The acoustic modes are overlapping, while the largest differences are in the optical modes, and probably are related to the exchange couplings between the top and bottom layers. Among other things, we highlight a breaking of the degeneracies, due to some proximity effect of the molecule. Moreover, we notice that the group velocity in $\Gamma \rightarrow K$ reduces by 0.5% after the adsorption.

9.4 Energy Method

For completeness, we report the results obtained following the energy method route introduced in Section 2.3.2. The idea behind the energy method is to calculate the ground-state energy of different magnetic configurations and to map them into the respective Heisenberg Hamiltonian with the spin values expressed with respect to the selected magnetic configuration. The magnetic configurations can be single atom spin-flip configurations, or different atoms rows spin-flip configurations (phase method). The latter allows to obtain average values without worrying about periodic boundary conditions. For these reasons we followed the latter. This energy method has already been applied to the case of other spinterfaces [78, 79].

9.4.1 NiO bulk

In the case of NiO bulk the equations obtained from the solution of the mapping are the following

$$\begin{aligned} J_1, J_2 &= \frac{1}{16}(E_{AFI} - E_{FM}) \\ J_3 &= \frac{1}{48}(4E_{AFII} - E_{FM} - 3E_{AFI}) \end{aligned} \tag{9.6}$$

where FM is the ferromagnetic configuration, AFI the antiferromagnetic configuration along the $[001]$ direction, and $AFII$ the antiferromagnetic configuration along the $[111]$ direction (the magnetic ground state). The results are the ones in the Table 9.2, compared with the ones obtained from the magnetic force theorem method. Comparable

Table 9.2 Exchange couplings [meV] for the NiO bulk, evaluated using the energy method (EM) and the magnetic force theorem (MFT).

	EM	MFT
J1,J2	-0.42	0.12
J3	-10.91	-9.02

results are obtained with a different effective U in [159]. The J3 seems sufficiently similar (20%) between the two methods. The J1, J2, instead differ even in the sign; however, these exchange couplings are very small and easily dependent on the numerical setup. Moreover, they are not significant in terms of the magnetic nature of the system.

9.4.2 FePc/NiO(001)

For the NiO(001) substrate, the Heisenberg Hamiltonian considered is the one of the supercell tri-layer, assuming J1 and J2 equal to zero in each layer and between the layers. Evaluating this for our $((6,0),(3,3))$ supercell but keeping the same periodicity as in the 1×1 cell yields (averaging of the exchange couplings)

$$H = -36(J3)_{12}S_1S_2 - 36(J3)_{34}S_3S_4 - 36(J3)_{56}S_5S_6 - 18(J3)_{16}S_1S_6 - 18(J3)_{25}S_2S_5 + E_0 \tag{9.7}$$

where each pair $(1,2)$, $(3,4)$, $(5,6)$ represents the rows of atoms of different magnetization in the ground state configuration for the different layers, respectively top, middle and bottom layer, as reported in Fig. 9.10.

The magnetic configurations considered are reported in Table. 9.3.

The NiO(001) results and the FePc/NiO(001) results are the ones in Table 9.4. This allows us to see if the conclusions obtained through the magnetic force theorem, can be obtained through this extremely simplified energy method. While the energy method partially reproduces the increase of the exchange coupling at the top and its decrease at the bottom, it does not give the expected decrease between the top and the bottom. Enlarging the Heisenberg Hamiltonian considered, does not solve this problem, and make the mapping quite more demanding. We notice the fact that in the pristine substrate the J3 at the top layer and bottom one are different, this is due to the fact that the bottom layer is fixed to be bulk-like.

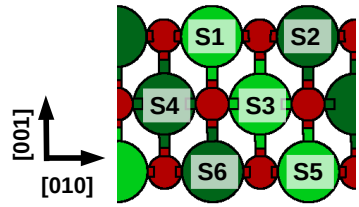

Figure 9.10 Side-view of the NiO(001), underlining the rows considered in the energy method mapping.

Table 9.3 Spin configurations considered in the mapping between the DFT calculations and the Heisenberg model in 9.7.

configurations	S_1	S_2	S_3	S_4	S_5	S_6
1	1	-1	1	-1	1	-1
2	1	-1	1	-1	-1	1
3	1	1	1	-1	1	-1
4	1	-1	1	1	1	-1
5	1	-1	1	-1	1	1
6	-1	1	1	1	1	1

Table 9.4 Energy method: comparison between the exchange couplings of the supercell with and without the molecule. In the Heisenberg Hamiltonian the J1 and J2 couplings have been considered equal to zero. Moreover, different magnetic phases have been considered instead of single atoms spin flips.

		Substrate	**Substrate+Molecule [meV]**
Intra-layers			
Top	J3	-9.96	-10.56
Middle	J3	-12.44	-12.38
Bottom	J3	-9.45	-9.07
Inter-layers			
Top-Bottom	J3	-7.81	-8.45

9.5 Conclusions

Although the effects induced by the adsorption of FePc on the substrate magnonic properties are marginal, we have obtained some hints about the possible chemical tuning of them through molecular adsorption.

The adsorption of the molecule induces a shift in the electronic charge distribution, moving it from the O atoms towards the transition-metal atoms. As underlined in the conclusions of Chapter 4, this movement is the result of two movements, one of the interface charge (mainly of O character) towards the molecule, the other of the charge shared in the pristine substrate between the surface O atoms and transition-metal atoms towards the latter.

This charge shift can affect the local magnetic moments of the transition-metal atoms, increasing or decreasing them based on factors such as the filling of d orbitals, the local exchange splitting, and crystal field splitting. In substrates like NiO and CoO, the increased electron density on the transition-metal atoms results in a decrease in their local magnetic moments. While the reduction in the magnetic moments is related to a decrease in the super-exchange coupling, the decrease of the O atom charge is related to an increase of it. For systems such as FePc/NiO and C60/CoO [39], the reduction in the magnetic moments of the transition-metal atoms is offset by a decrease in the charge on the O atoms, leading to a net increase in the surface super-exchange couplings. It's reasonable to assume that FePc on CoO(001) would exhibit similar behavior. However, as discussed in Chapter 4, FePc adsorption on CoO(001) is unique. Unlike the FePc/NiO(001) spinterface, the orbital contribution to magnetism plays a major role in the CoO system, complicating the interpretation of changes in the super-exchange couplings. Therefore, while these conclusions suggest pathways for chemically tuning magnonic properties, further studies focusing on the orbital component would be necessary to fully understand the FePc/CoO(001) spinterface.

Outlook

From these studies the complexity of the spinterface problem emerges: a significant dependence of the energetic, electronic, magnetic and optical characteristics with respect to the substrate considered has been highlighted. However, in spite of the peculiarities, we can extract some similarities, also in the perspective of applications.

The spinterfaces in the case of energetically-magnetically stable substrates mainly involve the first layers of the substrate, e.g. in NiO as reported in Fig. 8.3 and Cr_2O_3 Cr-terminated in Fig. 6.5. The bonding of Fe-phthalocyanine can be guided by the Fe atom, as in NiO (Fig. 8.3), or by the N atoms as in Cr_2O_3 Cr-terminated (Fig. 6.4), or by the two of them, as in Cr_2O_3 O-terminated (Fig. 7.6). Local modifications of magnetism can be observed at the bonding points. Orbitals of the molecule pointing toward the substrate are the most hybridized ones, e.g. the dz2, dxz and dyz orbitals of the Fe atom in NiO (Fig. 8.5). Light excitation produces movement of charge from the substrate towards the center of the molecule, e.g. in CoO (Fig. 4.5). The breaking of the spin symmetry of the substrate due to the molecule adsorption, makes the charge movement spin-unbalanced, as clearly shown in Cr_2O_3 Cr-terminated (Fig. 6.6).

Between these similarities, the possibility to produce through light excitation a spin-unbalanced charge movement is the one characteristic needed in the perspective of activate the spinterfaces to produce coherent spin excitations. In fact, as clearly shown in the case of NiO (Fig. 9.7), the local charge and magnetic variations are related to local variations in the magnetic couplings of the substrate, which define the dispersion of the coherent spin excitations.

The control of this activation requires deeper analysis of the optical spectra of the spinterfaces. In this regard, tight-binding models, extracted from the ab-initio results, could be used to obtain higher accuracy optical spectra of these large systems, at a lower computational cost, as introduced in the Appendix B.

Among other things, prior to the light activation problem, it is not to be forgotten that there are still difficulties related to the ground-state itself. The energetic proximity of numerous magnetic configurations, in fact, makes difficult to find the proper ground-state, as we underlined in Section 7.5. We are still working on finding new ways to solve this problem.

Lastly, with regard to the spinterfaces to consider with the goal of light activating them, we underline three points. First a major hybridization between the molecule and the substrate would be preferential, in order to maximise the effects of the light excitation of the molecule on the magnetic couplings of the substrate. Second, and related to the first, to have an effect on the magnetic couplings of the substrate, the hybridization has to be spin-unbalanced. In this regard an adsorption configuration breaking the spin

symmetry of the substrate is sufficient, and a magnetic molecule is not required. Third, the tunability of the spinterface is related to the presence of a molecular character and a substrate character, so the hybridization has not to be so that the two can not be distinguished anymore, at least if we are interested in a predictable response. This in terms of light excitation spectrum translates into the presence of high-intensity transitions with states of clear molecular character and substrate character.

Among the spinterfaces studied, some exhibit favorable properties from one perspective but fall short from another. For example, FePc/CoO(001) (Chapter 4) shows high-intensity substrate-molecule optical transitions, yet lacks spin-unbalance. Differently, FePc/Cr2O3(0001) with O-terminated surface (Chapter 7) displays noticeable substrate-molecule hybridization, but does not feature high-intensity substrate-molecule optical transitions. FePc/NiO(001) (Chapter 8) demonstrates low levels of both hybridization and spin-unbalance, making it less promising overall. The standout spinterface is FePc/Cr2O3(0001) with Cr-terminated surface (Chapter 6), which exhibits significant hybridization, spin-unbalance, and clear high-intensity substrate-molecule transitions, making it the most promising candidate in terms of optical tunability of the magnetic properties.

APPENDIX A

Group theory and Magnons

We believe that a better understanding of the magnonic problem can be obtained trough a topological approach and an ab-initio one. In order to follow the former route, it is necessary to introduce a few concepts of group theory.

A.1 Basic group theory notions

A group is a set of elements $G = \{a, b, c \dots\}$ which satisfies the following conditions

- the product between any two elements is also a group element $a \cdot b \in G$
- the product is associative $a \cdot (b \cdot c) = (a \cdot b) \cdot c$
- there is a unit element $e \in G$ such that $a \cdot e = a \; \forall a \in G$
- each element has an inverse element $a \cdot a^{-1} = a^{-1} \cdot a = e \; \forall a \in G$

A Class is the set of elements of the Group b that can be obtained from any element of the Group a by conjugation with a suitable element of the Group x

$$b = x^{-1} \cdot a \cdot x \tag{A.1}$$

A class represents the set of indistinguishable operations, as in the group D_{3h} the 3 rotations+reflections operations σ_v, that can be distinguished only by fixing an arbitrary reference system.

The one-to-one identification of the elements of the group G with matrices, is called a representation of the group G if the product operation is preserved (isomorphism)

$$M(a \cdot b) = M(a)M(b) \tag{A.2}$$

The dimensionality of a representation is equal to the dimensionality of its matrices.

The representation is reducible if all the matrices associated to the group elements can be brought to the same diagonal-block form by a single unitary transformation, or in other words, that the representation can be described as the direct product of different representations with lower dimensionalities.

Being the characters (traces) of the matrices defined modulo a unitary transformation, a representation is identified by the characters of the matrices. The characters of the elements of the same Class are equal. The characters allow to easily manipulate the representations of a Group, see for example [162].

A.2 Real-space band representation

Let us consider a coordinate $\boldsymbol{q}$, also called center, in the Wigner-Seitz cell and the associated symmetry space group $G_{\boldsymbol{q}}$ composed of those operations, indicated as $\{\gamma|\boldsymbol{\tau}\}$, which leave $\boldsymbol{q}$ invariant (apart for a Bravais lattice vector $\boldsymbol{R}$)

$$\{\gamma|\boldsymbol{\tau}\}\boldsymbol{q} = \boldsymbol{q} + \boldsymbol{R}_{\boldsymbol{q}}^{\{\gamma|\boldsymbol{\tau}\}} \tag{A.3}$$

where γ is a point-Group operation and $\boldsymbol{\tau}$ a translation operation. Let us denote by $g_{\boldsymbol{q}}$ the point group associated with the space group $G_{\boldsymbol{q}}$, i.e. the set of operations of the form $\{\gamma|\boldsymbol{0}\}$, and by $D^{(l)}(\gamma)$ its irreducible representations, where the index l ranges between 1 and the number of irreducible representations (equal to the number of classes of the point group). Let us denote instead, by T the translations group, i.e. the set of operations of the form $\{0|\boldsymbol{\tau}\}$. If the space group $G_{\boldsymbol{q}}$ is factorizable into the associated point group $g_{\boldsymbol{q}}$ and translations group T, then it is called a symmorphic space group. As a consequence, the space group $G_{\boldsymbol{q}}$ can be mapped into the factor group $g_{\boldsymbol{q}}/T$ (which is isomorphic to the point group $g_{\boldsymbol{q}}$ itself). The factor group $g_{\boldsymbol{q}}/T$ is the set of equivalence classes defined by the point group operations up to a translations group operation. In terms of representation, any representation of a symmorphic space group $G_{\boldsymbol{q}}$ is uniquely identified by the pair of representations of the point group $g_{\boldsymbol{q}}$ and of the translations group T.

Therefore, considering the reciprocal lattice vectors $\boldsymbol{k}$ as labels which identify the irreducible representations of the translations group, we can then write the representation of any element of the space group $G_{\boldsymbol{q}}$ as

$$\{\gamma|\boldsymbol{\tau}\} : D^{(\boldsymbol{q},l)}[\{\gamma|\boldsymbol{\tau}\},\boldsymbol{k}] = e^{-i\boldsymbol{k}\cdot\boldsymbol{R}_{\boldsymbol{q}}^{\{\gamma|\boldsymbol{\tau}\}}} D^{l}(\gamma) \tag{A.4}$$

where the exponential is the (Abelian) representation of the translations group and D the matrix associated to the space group element $\{\gamma|\boldsymbol{\tau}\}$ in the representation $(\boldsymbol{q},l)$.

At this point, we can decompose the general space group G into the cosets of a space group $G_{\boldsymbol{q}}$ of a generic center $\boldsymbol{q}$ in the Wigner-Seitz cell

$$G = G_{\boldsymbol{q}} \cup \{\alpha_2|\boldsymbol{a_2}\}G_{\boldsymbol{q}} \cup \{\alpha_3|\boldsymbol{a_3}\}G_{\boldsymbol{q}} \cup \cdots + \{\alpha_s|\boldsymbol{a_s}\}G_{\boldsymbol{q}} = \cup_s\{\cup_{\rho\in G_{\boldsymbol{q}}}\{\alpha_s|\boldsymbol{a_s}\}\} \tag{A.5}$$

where $\{\alpha_s|\boldsymbol{a_s}\}$ (α_s point-group operation and a translations group operation) are those elements not belonging to $G_{\boldsymbol{q}}$, but belonging to G. This decomposition allows us to build a representation for the general space group starting from a representation of the space group of the generic center. In other terms, given a basis set $C_{i\boldsymbol{q}}^{(l)}$ for a l-representation of the space group $G_{\boldsymbol{q}}$, where the index i ranges between 1 and the dimension of the l-representation

$$\{\gamma|\boldsymbol{\tau}\}C_{i\boldsymbol{q}}^{(l)} = \sum_j D_{ji}^{(\boldsymbol{q},l)}[\{\gamma|\boldsymbol{\tau}\},\boldsymbol{k}]C_{j\boldsymbol{q}}^{(l)} \tag{A.6}$$

the set of elements

$$C_{i\boldsymbol{q}}^{(l)}, C_{i\boldsymbol{q}_2}^{(l)} = \{\alpha_2|\boldsymbol{a}_2\}C_{i\boldsymbol{q}}^{(l)}, \cdots, C_{i\boldsymbol{q}_s}^{(l)} = \{\alpha_s|\boldsymbol{a}_s\}C_{i\boldsymbol{q}}^{(l)}, \tag{A.7}$$

forms a basis set for the $(\boldsymbol{q},l)$-representation of the space group G. In this regard, let us consider an arbitrary element $\{a|\boldsymbol{\alpha}\}$ of the space group G, its matrix form in the representation $(\boldsymbol{q},l)$ is uniquely determined by the action on the respective basis set.

This action can be related to the action of a point group operation on the associated basis set representation l:

$$\begin{aligned} \{a|\boldsymbol{\alpha}\}C^{(l)}_{i\boldsymbol{q_m}} = \{a|\boldsymbol{\alpha}\}\{\alpha_m|\boldsymbol{a}_m\}C^{(l)}_{i\boldsymbol{q}} = \{\alpha_n|\boldsymbol{a}_n\}\{\gamma|\boldsymbol{c}\}C^{(l)}_{i\boldsymbol{q}} \\ = \{\alpha_n|\boldsymbol{a}_n\}\sum_j D^{(\boldsymbol{q},l)}_{ji}[\{\gamma|\boldsymbol{c}\}, a^{-1}\boldsymbol{k}]C^{(l)}_{j\boldsymbol{q}} = \sum_j D^{(\boldsymbol{q},l)}_{ji}[\{\gamma|\boldsymbol{c}\}, a^{-1}\boldsymbol{k}]C^{(l)}_{j\boldsymbol{q_n}}, \end{aligned} \tag{A.8}$$

Any element of G is in fact uniquely related to an element $\{\gamma|\boldsymbol{c}\}$ of $G_{\boldsymbol{q}}$ through the coset decomposition A.5

$$\{a|\boldsymbol{\alpha}\}\{\alpha_m|\boldsymbol{a}_m\} = \{\alpha_n|\boldsymbol{a}_n\}\{\gamma|\boldsymbol{c}\}. \tag{A.9}$$

Thus, the representations of G, also called band representations, can be found considering the irreducible representations of the centers in the Wigner-Seitz cell. In the specific, if we are interested in the irreducible band representations of G, the chosen centers in the Wigner-Seitz cell have to be relevant symmetry centers.

Two (symmetry) centers $\boldsymbol{q}_1$ and $\boldsymbol{q}_2$ are equivalent if their point groups $g_{\boldsymbol{q}_1} = g_{\boldsymbol{q}_2}$ and their translation factors coincide, for a Bravais lattice ($\boldsymbol{R}$) translation

$$e^{i\boldsymbol{k}\cdot\boldsymbol{R}^{(\gamma|\boldsymbol{c})}_{\boldsymbol{q}_2}} = e^{i\boldsymbol{k}\cdot\boldsymbol{R}}e^{i\boldsymbol{k}\cdot\boldsymbol{R}^{(\gamma|\boldsymbol{c})}_{\boldsymbol{q}_1}} \tag{A.10}$$

Two (symmetry) centers are called subequivalent if the point group of one is a subgroup of the others, and if all the translation factors of the two coincide a part a Bravais lattice translation. A center that is not subequivalent to any other center is called a relevant symmetry center or a Wyckoff-position of the space group G.

The irreducible band representations $(\boldsymbol{q}, l)$ of the space group G are generally called band representations (BR). BRs not unitarily equivalent to a direct sum of two or more BRs, are called elementary band representations (EBRs).

A band representation has information about the connectivity between different irreducible representations at different $\boldsymbol{k}$ points (little point groups $g_{\boldsymbol{k}}$ representations, where the little point group $g_{\boldsymbol{k}}$ is the set of operations which leave $\boldsymbol{k}$ invariant).

A set of r electronic bands, defined as the solutions to the electronic problem across all $\boldsymbol{k}$-points in the Brillouin zone (BZ), is said topologically non-trivial if it cannot be expressed as a direct sum of elementary band representations (EBRs) with non-negative integer coefficients. In other words, these bands cannot be constructed purely from localized atomic orbitals while respecting the crystal's symmetries.

Conversely, a set of electronic bands is said to be topologically trivial if it can be written as a direct sum of EBRs. Such a band structure can be smoothly deformed into an atomic limit, implying no non-trivial topological properties.

A few remarks about magnetic space groups are needed. In a magnetic space group G_M, the introduction of the time-reversal operator makes the usual definition of representation of the group not anymore possible, due to the fact that the group operation can not be preserved: generalized representations have to be defined, generally called co-representations. However, instead of working directly with the magnetic space group and its co-representations, it is common to work with the unitary part of the magnetic space group; in fact, the irreducible co-representations of the former are associated to the irreducible representations of the latter (the Dimmock-Wheeler test) [163, 164].

A.3 The magnonic bands

The set of operations which leave the Heisenberg Hamiltonian invariant form the group G_H. Its subgroup which leaves the magnetic ordering $\langle S^{\alpha}_i \rangle$ invariant is referred to as G_M.

If the (spin-orbit) coupling between the lattice and the localized moments is significant, the group G_M is a magnetic space group, if instead the coupling is weak, then the group G_M is a direct product of a lattice space group and a spin group, and identified as a spin space group.

Due to the linear relation between transverse spin operators and bosonic creation an annihilation operators, the symmetry considerations on the magnetic ground state reflect on the magnonic bands, i.e. G_M is the symmetry group of the magnonic bands.

Considering the Wyckoff positions of the magnetic ions and their magnetic point group g_M, the induced magnonic band representations (BRs) follow; fortunately, these are tabulated on the Bilbao Crystallographic Server [165, 166], in the section called MBANDREP (magnetic band representations). Of the different induced band representations only those associated to local irreducible representations of the transverse spin operators (the ones perpendicular to the quantization axis) are considered [167].

A.3.1 NiO bulk

NiO has a rock-salt structure, i.e space group $Fm\bar{3}m$ (point group $m\bar{3}m$, i.e. O_h). The magnetic space group preserving the AF ordering is C_c2/c (Schubnikov's Group IV, propagation vector $[1/2, 1/2, 1/2]$). Between the Wickoff positions of the magnetic space group, $4c$ is the one associated to the magnetic ion. The magnetic point group of the $4c$ position is $2'/m'$. In the group $2'/m'$ the irreducible representations associated to the transverse spin moments $\hat{S}^{\pm}$ are the two A_g representations (one is related to negative energy solutions of the magnonic problem, so it is here not considered). The band representation induced by the pair $(4c, A_g)$ is then $A_g \uparrow G(2)$. Two band representations are induced. These are degenerate in most of the special k-points of the BZ, apart $\Gamma(000)$ and $Y(010)$ (these breakdowns of the degeneracy can be caused by spin-orbit coupling or any external perturbation which is not changing the magnetic space group of the system, as reported in [168]).

APPENDIX B

The BSE Hamiltonian in a Wannier basis

Due to the importance in the absorption optical spectra of the screened electron-hole interaction and the related formation of excitonic states, it is necessary to go beyond the individual quasiparticle excitations and to solve the Bethe-Salpeter equation.

In order to reduce the computational effort of this task, an idea would be to consider a tight-binding model of the studied system and to solve the Bethe-Salpeter equation related to this model. This would allow us also to modify the model, adding contributions as spin-orbit coupling a posteriori, and to obtain the effects directly on the adsorption optical spectra. Notice that we would extract the tight-binding model through a Wannierisation procedure, as already done in Chapter 9.

The theoretical derivation which is the one reported in Section 2.3.1 assumes the orthonormality of the basis set of the tight-binding model. This condition could be avoided at a later stage, modifying the theoretical derivation and the implementation. These results are preliminary and major testing is still needed; however, also in the view of some perspectives, we find valuable to add them.

B.1 Literature survey

There are different studies trying to obtain BSE spectra from a tight-binding Hamiltonian [108, 169, 170]. One of the main differences in the codes by A. Dias et al. [169] and Uria-Alvares et al. [108] is the evaluation of the dipoles in transition space: in the former these are directly evaluated from the tight-binding Hamiltonian, in the latter the integrals over the Wannier functionas are instead considered and are approximated considering delta-like Wannier functions. The code by K. Merkel et al. [170] is different in this regard, because the excitonic problem is written in terms of the Wannier functions themselves and not in terms of optical transitions, making the evaluation of the dipoles in transition space not necessary. With the aim of implementing also magnetic systems and avoid delta-like approximation of the code by A. Dias et al, we started writing our own code. With respect to the codes cited above we are able to go beyond the Tamm-Dancoff approximation and to calculate the screening W at the RPA level. Howevere, due to computational effort, we evaluate the W as in the codes cited above, considering a homogeneous screening in reciprocal space. Among the other things, we can easily implement the possibility to consider $q \neq 0$ spectra. With respect to the code by Uria-Alvares et al. we can add non-local effects, i.e. reciprocal lattice vector different from 0 to the expansion of the coulomb potential. The extraction of a tight-binding model, despite its simplification and the introduction of some arbitrariness, could make the problem of calculating the optical spectra beyond IPA computationally accessible, also for system sizes like the ones we are considering.

B.2 Bulk silicon

We use bulk silicon as a first, simple test case for our BSE implementation which relies on Wannier functions.

In the case of bulk silicon, the bands around Fermi are of s and p characters. This means that a Wannierisation of these states can be quite susceptible to the choice of chosen parameters. Different tests have been done in the Wannierisation, in order to reduce the Wannier functions (WFs) spreading, to fit the energy bands and to reduce the ratio between imaginary and real parts of the Wannier functions. If the maximally-localized-Wannier functions are not real, than the spreading functional is in a local minimum [171].

While to consider a significant number of WFs with generic initial projectors (p+s+random projectors) allows to reduce significantly the spreading of the obtained WFs, preserving a good fitting of the DFT bands, it worsens significantly the ratio between the imaginary and real parts of the obtained WFs.

Proper initial projectors (s(on bonds)+sp3+random projectors) can help into reducing the ratio between the imaginary and real parts of the obtained WFs. However, to reach ratios of the order of 10^{-4}, less WFs in the Wannierisation procedure have to be considered, facilitating the finding of the global minimum of the spreading functional.

From the numerous tests we did, the two possible choices have emerged

- 16 WFs with initial projectors s(on bonds)+sp3+random, average spreading $\simeq 1.26$ Å^2, optimal fitting in the relevant subspace (4 valence + 4 conduction) and ratios of the order of 10^{-2};
- 8 WFs with initial projectors s(on bonds)+sp3, average spreading $\simeq 2.6$ Å^2, not-optimal fitting of the higher bands and ratios of the order of $\simeq 10^{-3}$.

To make the calculation quicker, an empirical dielectric constant (diagonal and static) ϵ^{-1} has been used; however, the implemented code has also the possibility to calculate it at the IPA and RPA order. Notice that to calculate W at the RPA order would require much more empty bands than the ones obtained here through the Wannierisation.

A value of 11.4 has been selected in the range of the different experimental values reported in the references [172–174].

In the Tamm-Dancoff approximation, with 1000 k points randomly chosen in the BZ, 2 conduction bands + 4 valence bands and the 8 WFs model, the spectra in Fig. B.2 are obtained. The BSE spectra reminds the experimental one; however, the two peaks at 3.5 eV and at 4.5 eV are not as high as expected. This is probably due to the approximations done: the W approximation and the dipole approximation. However, to consider the complete dipole makes the calculation computationally demanding. In this regard, one can truncate the screened coupling W, considering only the $\boldsymbol{k}$ points differences inside a fixed sphere. We implemented this possibility, and the user can enlarge the radius of the sphere, but the choice of the proper radius is not a straightforward choice. In fact, the spectra obtained considering 1000 k points, 2 conduction + 2 valence bands, real space integrals over a supercell $3 \times 3 \times 3$ and a radius of 0.2 Å^{-1}, are much worse (not reported here) than the one obtained with the above dipole approximation.

B.3 Bulk NiO

Let us consider the NiO with $U = 5.8$ eV, having already selected the proper parameters for the Wannierisation from the preceding studies of the magnetic couplings in Chapter 9. In this case the Wannierisation is easier than in the silicon case, having mainly d

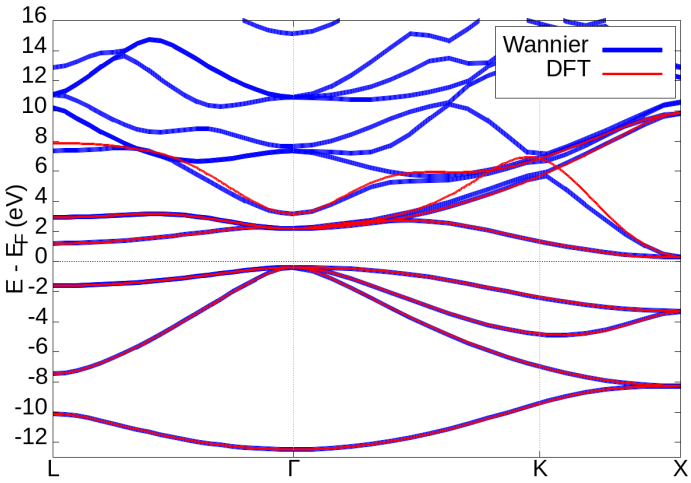

Figure B.1 Electronic band structure of Si bulk. Solid/dash-dotted lines indicate DFT and Wannier results, respectively. The position of the Fermi energy in the gap is arbitrary. The following are the considered parameters: frozen window $\simeq (-\infty, E_F + 3]$, larger window $\simeq (-\infty, E_F + 13]$, initial projectors s(on bonds)+sp3, 20 iterations in the maximal-localization procedure.

and p orbitals. This translates in terms of the spectra also in the need of a less significant number of k points, having less dispersive bands.

As initial projectors p orbitals for the O atoms and d orbitals for the Ni atoms have been considered. In order to reduce the ratio between the real part and the imaginary part of the WFs ($\simeq 0.0025$), the frozen window and the larger window have been chosen respectively equal to $(\infty, E_F]$ and $(\infty, E_F + 11]$ eV. The average spreading of the simil-d orbitals is 1.48 Å^2, while the one of the simil-p orbitals is 3.22 Å^2.

To fasten the calculations an empirical dielectric constant of 11.9 [175] has been considered.

Considering the Tamm-Dancoff (TD) approximation, 400 k points randomly chosen in the BZ, 2 conduction and 8 valence bands, the spectra in Fig. B.3 are obtained. The interpretation of these results is not straightforward, due to the fact that here we are considering only transitions involving the conduction bands of d character. There is no similarity between the experimental data and the BSE-TD spectra, while the IPA spectra reproduces well what already reported in the literature [11]. However, the addition of a normalization of $1/(6\pi)$ has been needed to obtain a comparable IPA. This suggests that the code needs more testing, as already suggested by the Si studies.

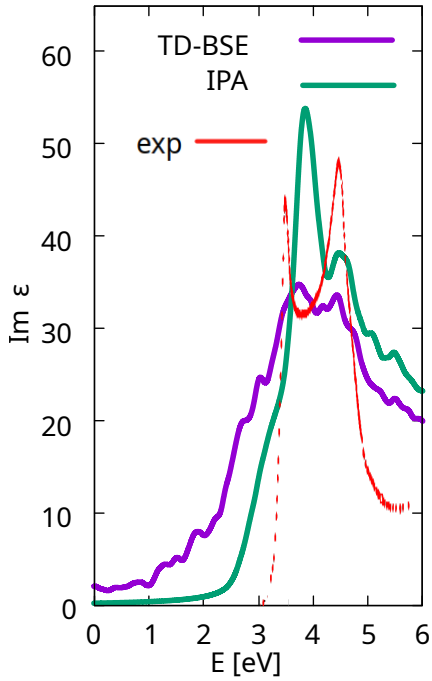

Figure B.2 Si: BSE (Tamn-Dancoff) and IPA adsorption spectra of the 8WFs model Hamiltonian (polarization averaged over the x,y and z directions). The dipoles for this calculation are calculated with the approximated-method. A Lorenzian broadening of 0.1 eV has been considered. In red the experimental data reported from [10].

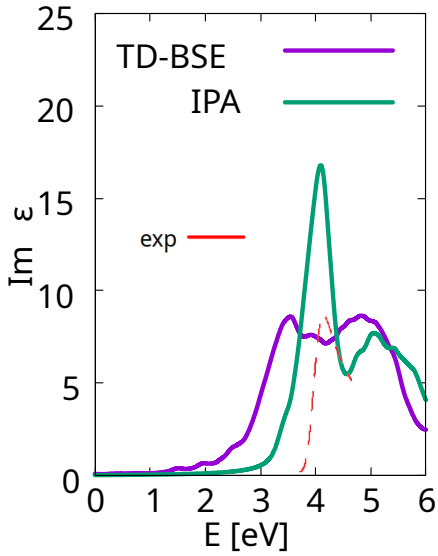

Figure B.3 NiO: BSE (Tamn-Dancoff) and IPA adsorption spectra (polarization averaged over the x, y, and z directions). The dipoles for this calculation are calculated with the approximated-method. A Lorenzian broadening of 0.1 eV has been considered. In red the experimental data reported from [11]. A factor $1/(6\pi)$ has been considered to make the IPA spectra comparable to the literature results [11].

Bibliography

[1] Igor Žutić, Jaroslav Fabian, and S. Das Sarma. Spintronics: Fundamentals and applications. *Rev. Mod. Phys.*, 76:323–410, Apr 2004. doi: 10.1103/RevModPhys.76.323.

[2] Stefano Sanvito. The rise of spinterface science. *Nature Physics*, 6(8):562–564, 2010. doi: 10.1038/nphys1714.

[3] Mattia Benini, Giuseppe Allodi, Alessandro Surpi, Alberto Riminucci, Ko-Wei Lin, Samuele Sanna, Valentin Alek Dediu, and Ilaria Bergenti. In-depth NMR investigation of the magnetic hardening in Co thin films induced by the interface with molecular layers. *Advanced Materials Interfaces*, 9(36):2201394, 2022. doi: 10.1002/admi.20220139.

[4] Giulia Avvisati, Claudia Cardoso, Daniele Varsano, Andrea Ferretti, Pierluigi Gargiani, and Maria Grazia Betti. Ferromagnetic and antiferromagnetic coupling of spin molecular interfaces with high thermal stability. *Nano letters*, 18(4):2268–2273, 2018. doi: 10.1021/acs.nanolett.7b04836.

[5] Peisen Yuan, Sara Catalano, Witold Skowronski, Roger Llopis, Fèlix Casanova, and Luis E. Hueso. Tuning the magnon transport properties of y3fe5o12 with a cobalt phthalocyanine molecular layer. *ACS Applied Electronic Materials*, 6(6):4232–4238, 2024. doi: 10.1021/acsaelm.4c00332.

[6] Henning Maximilian Sturmeit, Iulia Cojocariu, Andreas Windischbacher, Peter Puschnig, Cinthia Piamonteze, Matteo Jugovac, Alessandro Sala, Cristina Africh, Giovanni Comelli, Albano Cossaro, Alberto Verdini, Luca Floreano, Matus Stredansky, Erik Vesselli, Chantal Hohner, and Miroslav Kettner et al. Room-temperature on-spin-switching and tuning in a porphyrin-based multifunctional interface. *Small*, 17(50):2104779, 2021. doi: 10.1002/smll.202104779.

[7] Dorye L Esteras, Andrey Rybakov, Alberto M Ruiz, and José J. Baldoví. Magnon straintronics in the 2d van der waals ferromagnet CrSBr from first-principles. *Nano Letters*, 22(21):8771–8778, 2022. doi: 10.1021/acs.nanolett.2c02863.

[8] Hongo K. Ichibha T., Hou Z. and Maezono R. New insight into the ground state of FePc: A diffusion Monte Carlo study. *Scientific reports*, 7(1):2011, 2017. doi: 10.1038/s41598-017-01668-6.

[9] Alan Kramer, Luca Bignardi, Paolo Lacovig, Silvano Lizzit, and Matthias Batzill. Comparison of surface structures of corundum Cr2O3(0001) and V2O3(0001) ultrathin films by x-ray photoelectron diffraction. *Journal Of Physics: Condensed Matter*, 30(7):074002, 2018. doi: 10.1088/1361-648X/aaa5ed.

[10] P. Lautenschlager, Miquel Garriga, L Vina, and Manuel Cardona. Temperature dependence of the dielectric function and interband critical points in silicon. *Physical Review B*, 36(9):4821, 1987.

[11] Claudia Rödl and Friedhelm Bechstedt. Optical and energy-loss spectra of the antiferromagnetic transition metal oxides MnO, FeO, CoO, and NiO including quasiparticle and excitonic effects. *Physical Review B—Condensed Matter and Materials Physics*, 86(23):235122, 2012. doi: 10.1103/PhysRevB.86.235122.

[12] A. Rohrbach, J. Hafner, and G. Kresse. Ab initio study of the (0001) surfaces of hematite and chromia: Influence of strong electronic correlations. *Physical Review B*, 70:125426–, 09 2004. doi: 10.1103/PhysRevB.70.125426.

[13] M Catti, G Sandrone, G Valerio, and R Dovesi. Electronic, magnetic and crystal structure of Cr2O3 by theoretical methods. *Journal of Physics and Chemistry of Solids*, 57(11):1735–1741, 1996. doi: 10.1016/0022-3697(96)00034-0.

[14] Jagadeesh S. Moodera and George Mathon. Spin polarized tunneling in ferromagnetic junctions. *Journal of Magnetism and Magnetic Materials*, 200(1):248–273, 1999. ISSN 0304-8853. doi: 10.1016/S0304-8853(99)00515-6.

[15] Evgeny Y Tsymbal, Oleg N Mryasov, and Patrick R LeClair. Spin-dependent tunnelling in magnetic tunnel junctions. *Journal of Physics: Condensed Matter*, 15(4): R109, 2003. doi: 10.1088/0953-8984/15/4/201.

[16] Hiroyoshi Itoh and Jun-ichiro Inoue. Theory of tunnel magnetoresistance. *Journal of the Magnetics Society of Japan*, 30(1):1–37, 2006. doi: 10.3379/jmsjmag.30.1.

[17] Robert L White. Giant magnetoresistance: A primer. *IEEE transactions on Magnetics*, 28(5):2482–2487, 1992. doi: 10.1109/20.179533.

[18] Evgeny Y Tsymbal and David G Pettifor. Perspectives of giant magnetoresistance. In *Solid state physics*, volume 56, pages 113–237. Elsevier, 2001.

[19] Georg Martin Müller. *Spin dynamics of equilibrium electrons in gallium arsenide*. PhD thesis, 2010.

[20] Y Yafet. g factors and spin-lattice relaxation of conduction electrons. In *Solid state physics*, volume 14, pages 1–98. Elsevier, 1963.

[21] Lénárd Szolnoki, Balázs Dóra, Annamária Kiss, Jaroslav Fabian, and Ferenc Simon. Intuitive approach to the unified theory of spin relaxation. *Physical Review B*, 96(24):245123, 2017. doi: 10.1103/PhysRevB.96.245123.

[22] Michel Dyakonov and V.I. Perel. *CHAPTER 2. Theory of Optical Spin Orientation of Electrons and Nuclei in Semiconductors*, volume 8, pages 11–71. Modern Problems in Condensed Matter Sciences, 12 1984. ISBN 9780444867414. doi: 10.1016/B978-0-444-86741-4.50007-X.

[23] Jens Hübner, WW Rühle, M Klude, D Hommel, RDR Bhat, JE Sipe, and HM Van Driel. Direct observation of optically injected spin-polarized currents in semiconductors. *Physical review letters*, 90(21):216601, 2003. doi: 10.1103/PhysRevLett.90.216601.

[24] S. Pfalz, R. Winkler, T. Nowitzki, D. Reuter, A. D. Wieck, D. Hägele, and M. Oestreich. Optical orientation of electron spins in gaas quantum wells. *Phys. Rev. B*, 71: 165305, Apr 2005. doi: 10.1103/PhysRevB.71.165305.

[25] Xi Chen, Tengfei Yan, Bairen Zhu, Siyuan Yang, and Xiaodong Cui. Optical control of spin polarization in monolayer transition metal dichalcogenides. *ACS nano*, 11 (2):1581–1587, 2017. doi: 10.1021/acsnano.6b07061.

[26] WJM Naber, S Faez, and Wilfred Gerard van der Wiel. Organic spintronics. *Journal of Physics D: Applied Physics*, 40(12):R205, 2007. doi: 10.1088/0022-3727/40/12/

R01.

[27] Jagannath Devkota, Rugang Geng, Ram Chandra Subedi, and Tho Duc Nguyen. Organic spin valves: a review. *Advanced Functional Materials*, 26(22):3881–3898, 2016. doi: 10.1002/adfm.201504209.

[28] V. Dediu, M. Murgia, F.C. Matacotta, C. Taliani, and S. Barbanera. Room temperature spin polarized injection in organic semiconductor. *Solid State Communications*, 122(3):181–184, 2002. ISSN 0038-1098. doi: 10.1016/S0038-1098(02)00090-X.

[29] Clément Barraud, Pierre Seneor, Richard Mattana, Stéphane Fusil, Karim Bouzehouane, Cyrile Deranlot, Patrizio Graziosi, Luis Hueso, Ilaria Bergenti, Valentin Dediu, et al. Unravelling the role of the interface for spin injection into organic semiconductors. *Nature Physics*, 6(8):615–620, 2010. doi: 10.1038/nphys1688.

[30] Stefano Sanvito. Molecular spintronics. *Chemical Society Reviews*, 40(6):3336–3355, 2011. doi: 10.1039/C1CS15047B.

[31] Ilaria Bergenti and Valentin Dediu. Spinterface: A new platform for spintronics. *Nano Materials Science*, 1(3):149–155, 2019. doi: 10.1016/j.nanoms.2019.05.002.

[32] Mirko Cinchetti, V. Alek Dediu, and Luis E. Hueso. Activating the molecular spinterface. *Nature Materials*, 16:507–515, 2017. doi: 10.1038/nmat4902.

[33] Ferdinand Huber, Julian Berwanger, Svitlana Polesya, Sergiy Mankovsky, Hubert Ebert, and Franz J Giessibl. Chemical bond formation showing a transition from physisorption to chemisorption. *Science*, 366(6462):235–238, 2019. doi: 10.1126/science.aay3444.

[34] JK Norskov. Chemisorption on metal surfaces. *Reports on Progress in Physics*, 53 (10):1253, 1990. doi: 10.1088/0034-4885/53/10/001.

[35] GG Kleiman and Uzi Landman. Theory of physisorption: He on metals. *Physical Review B*, 8(12):5484, 1973. doi: 10.1103/PhysRevB.8.5484.

[36] Antoni Franco-Cañellas, Steffen Duhm, Alexander Gerlach, and Frank Schreiber. Binding and electronic level alignment of π-conjugated systems on metals. *Reports on Progress in Physics*, 83(6):066501, 2020. doi: 10.1088/1361-6633/ab7a42.

[37] Kaushik Bairagi, Amandine Bellec, Vincent Repain, C Chacon, Y Girard, Yves Garreau, J Lagoute, S Rousset, R Breitwieser, Yu-Cheng Hu, et al. Tuning the magnetic anisotropy at a molecule-metal interface. *Physical review letters*, 114(24):247203, 2015. doi: 10.1103/PhysRevLett.114.247203.

[38] Federico Orlando, Guido Fratesi, Giovanni Onida, and Simona Achilli. Tailoring the magnetic ordering of the Cr4O5/Fe(001) surface via a controlled adsorption of C60 organic molecules. *Physical Chemistry Chemical Physics*, 23(13):7948–7954, 2021. doi: 10.1039/D0CP05848C.

[39] Luca Gnoli, Mattia Benini, Corrado Del Conte, Alberto Riminucci, Rajib K Rakshit, Manju Singh, Samuele Sanna, Roshni Yadav, Ko-Wei Lin, Alessio Mezzi, et al. Enhancement of magnetic stability in antiferromagnetic coo films by adsorption of organic molecules. *ACS Applied Electronic Materials*, 2024. doi: 10.1021/acsaelm.3c01599.

[40] J. Michael Gottfried. Surface chemistry of porphyrins and phthalocyanines. *Surface Science Reports*, 70:259–379, 2015. doi: 10.1016/j.surfrep.2015.04.001.

[41] Meng-Sheng Liao and Steve Scheiner. Electronic structure and bonding in metal porphyrins, metal= Fe, Co, Ni, Cu, Zn. *The Journal of chemical physics*, 117(1):205–219, 2002. doi: 10.1063/1.1480872.

[42] Meng-Sheng Liao and Steve Scheiner. Electronic structure and bonding in metal phthalocyanines, metal= Fe, Co, Ni, Cu, Zn, Mg. *The Journal of Chemical Physics*,

114(22):9780–9791, 2001. doi: 10.1063/1.1367374.

[43] Lapo Bogani and Wolfgang Wernsdorfer. Molecular spintronics using single-molecule magnets. *Nature materials*, 7(3):179–186, 2008. doi: 10.1038/nmat2133.

[44] Richard A Layfield. Organometallic single-molecule magnets. *Organometallics*, 33 (5):1084–1099, 2014. doi: 10.1021/om401107f.

[45] Daniel N Woodruff, Richard EP Winpenny, and Richard A Layfield. Lanthanide single-molecule magnets. *Chemical reviews*, 113(7):5110–5148, 2013. doi: 10.1021/cr400018q.

[46] A Lodi Rizzini, C Krull, Timofey Balashov, JJ Kavich, Aitor Mugarza, Piter S Miedema, Pardeep K Thakur, Violetta Sessi, Svetlana Klyatskaya, Mario Ruben, et al. Coupling single molecule magnets to ferromagnetic substrates. *Physical review letters*, 107(17):177205, 2011. doi: 10.1103/PhysRevLett.107.177205.

[47] Alberto Lodi Rizzini, Cornelius Krull, Aitor Mugarza, Timofey Balashov, Corneliu Nistor, Raoul Piquerel, Svetlana Klyatskaya, Mario Ruben, Polina M Sheverdyaeva, Paolo Moras, et al. Coupling of single, double, and triple-decker metal-phthalocyanine complexes to ferromagnetic and antiferromagnetic substrates. *Surface Science*, 630:361–374, 2014. doi: 10.1016/j.susc.2014.07.008.

[48] Gruber Manuel et al. Exchange bias and room-temperature magnetic order in molecular layers. *Nature materials*, 14(10):981–984, 2015. doi: 10.1038/nmat4361.

[49] Warner Ben et al. Tunable magnetoresistance in an asymmetrically coupled single-molecule junction. *Nature nanotechnology*, 10(3):259–263, 2015. doi: 10.1038/nnano.2014.326.

[50] Warner Marc et al. Potential for spin-based information processing in a thin-film molecular semiconductor. *Nature*, 7477:504–508, 2013. doi: 10.1038/nature12597.

[51] Trashin Stanislav et al. Singlet oxygen-based electrosensing by molecular photosensitizers. *Nature communications*, 8(1):16108, 2017. doi: 10.1038/ncomms16108.

[52] Zhang X. et al. Zhang X., Wu Z. Highly selective and active co2 reduction electrocatalysts based on cobalt phthalocyanine/carbon nanotube hybrid structures. *Nature communications*, 8:14675, 2017. doi: 10.1038/ncomms14675.

[53] Forrer D. et al. Sedona F., Di Marino M. Tuning the catalytic activity of ag(110)-supported fe phthalocyanine in the oxygen reduction reaction. *Nature Mater*, 11: 970–977, 2012. doi: 10.1021/acscatal.2c03298.

[54] Wenmu Li, Aiping Yu, Drew C. Higgins, Bernard G. Llanos, and Zhongwei Chen. Biologically inspired highly durable iron phthalocyanine catalysts for oxygen reduction reaction in polymer electrolyte membrane fuel cells. *Journal of the American Chemical Society*, 132(48):17056–17058, 2010. doi: 10.1021/ja106217u.

[55] Cao Ruiguo et al. Promotion of oxygen reduction by a bio-inspired tethered iron phthalocyanine carbon nanotube-based catalyst. *Nature communications*, 4(1):2076, 2013. doi: 10.1038/ncomms3076.

[56] Dan Sun, Yue Shen, Wang Zhang, Ling Yu, Ziqi Yi, Wei Yin, Duo Wang, Yunhui Huang, Jie Wang, Deli Wang, and John B. Goodenough. A solution-phase bifunctional catalyst for lithium–oxygen batteries. *Journal of the American Chemical Society*, 136(25):8941–8946, 2014. doi: 10.1021/ja501877e.

[57] C. Grazia Bezzu, Madeleine Helliwell, John E. Warren, David R. Allan, and Neil B. McKeown. Heme-like coordination chemistry within nanoporous molecular crystals. *Science*, 327(5973):1627–1630, 2010. doi: 10.1126/science.1184228.

[58] John R. et al. Tritsch. Harvesting singlet fission for solar energy conversion via triplet energy transfer. *Nature communications*, 4(1):2679, 2013. doi: 10.1038/

ncomms3679.

[59] Kongchao Shen, Bai Narsu, Gengwu Ji, Haoliang Sun, Jinbang Hu, Zhaofeng Liang, Xingyu Gao, Haiyang Li, Zheshen Li, Bo Song, et al. On-surface manipulation of atom substitution between cobalt phthalocyanine and the cu (111) substrate. *RSC advances*, 7(23):13827–13835, 2017. doi: 10.1039/C7RA00636E.

[60] S. Stepanow, P. S. Miedema, A. Mugarza, G. Ceballos, P. Moras, J. C. Cezar, C. Carbone, F. M. F. de Groot, and P. Gambardella. Mixed-valence behavior and strong correlation effects of metal phthalocyanines adsorbed on metals. *Phys. Rev. B*, 83: 220401, Jun 2011. doi: 10.1103/PhysRevB.83.220401.

[61] P. Palmgren, T. Angot, C. I. Nlebedim, J.-M. Layet, G. Le Lay, and M. Göthelid. Ordered phthalocyanine superstructures on Ag(110). *The Journal of Chemical Physics*, 128(6):064702, 02 2008. ISSN 0021-9606. doi: 10.1063/1.2827864.

[62] Heiko Peisert, Johannes Uihlein, Fotini Petraki, and Thomas Chassé. Charge transfer between transition metal phthalocyanines and metal substrates: The role of the transition metal. *Journal of Electron Spectroscopy and Related Phenomena*, 204:49–60, 2015. doi: 10.1016/j.elspec.2015.01.005.

[63] F. Djeghloul et al. Direct observation of a highly spin-polarized organic spinterface at room temperature. *Scientific Reports*, 3, 2013. doi: 10.1038/srep01272.

[64] John Åhlund, Joachim Schnadt, Katharina Nilson, Emmanuelle Göthelid, Joachim Schiessling, Flemming Besenbacher, Nils Mårtensson, and Carla Puglia. The adsorption of iron phthalocyanine on graphite: a scanning tunnelling microscopy study. *surface science*, 601(17):3661–3667, 2007. doi: 10.1016/j.susc.2007.06.008.

[65] David Maximilian Janas, Andreas Windischbacher, Mira Sophie Arndt, Michael Gutnikov, Lasse Sternemann, David Gutnikov, Till Willershausen, Jonah Elias Nitschke, Karl Schiller, Daniel Baranowski, et al. Metalloporphyrins on oxygen-passivated iron: Conformation and order beyond the first layer. *Inorganica Chimica Acta*, 557:121705, 2023. doi: 10.1016/j.ica.2023.121705.

[66] M. Bernien, J. Miguel, C. Weis, Md. E. Ali, J. Kurde, B. Krumme, Pooja M. Panchmatia, B. Sanyal, M. Piantek, P. Srivastava, et al. Tailoring the nature of magnetic coupling of fe-porphyrin molecules to ferromagnetic substrates. *Physical review letters*, 102(4):047202, 2009. doi: 10.1103/PhysRevLett.102.047202.

[67] Margareta Wagner, Fabio Calcinelli, Andreas Jeindl, Michael Schmid, Oliver T Hofmann, and Ulrike Diebold. Adsorption configurations of Co-phthalocyanine on In2O3(111). *Surface Science*, 722:122065, 2022. doi: 10.1016/j.susc.2022.122065.

[68] Reimer Karstens, Thomas Chassé, and Heiko Peisert. Interface interaction of transition metal phthalocyanines with strontium titanate (100). *Beilstein Journal of Nanotechnology*, 12(1):485–496, 2021. doi: 10.3762/bjnano.12.39.

[69] Lingyun Liu, Wenhua Zhang, Panpan Guo, Kai Wang, Jiaou Wang, Haijie Qian, Ibrahim Kurash, Chia-Hsin Wang, Yaw-Wen Yang, and Faqiang Xu. A direct Fe-O coordination at the FePc/MoOx interface investigated by XPS and NEXAFS spectroscopies. *Physical Chemistry Chemical Physics*, 17(5):3463–3469, 2015. doi: 10.1039/C4CP04199B.

[70] Reimer Karstens, Mathias Glaser, Axel Belser, David Balle, Małgorzata Polek, Ruslan Ovsyannikov, Erika Giangrisostomi, Thomas Chassé, and Heiko Peisert. Fepc and fepcf16 on rutile tio2 (110) and (100): influence of the substrate preparation on the interaction strength. *Molecules*, 24(24):4579, 2019. doi: 10.3390/molecules24244579.

[71] Tobias Schmitt, Pascal Ferstl, Lutz Hammer, M. Alexander Schneider, and Josef Redinger. Adsorption and intermolecular interaction of cobalt phthalocyanine on

CoO(111) ultrathin films: An STM and DFT study. *The Journal of Physical Chemistry C*, 121(5):2889–2895, 2017. doi: 10.1021/acs.jpcc.6b12337.

[72] Mathias Glaser, Heiko Peisert, Hilmar Adler, Małgorzata Polek, Johannes Uihlein, Peter Nagel, Michael Merz, Stefan Schuppler, and Thomas Chasse. Transition-metal phthalocyanines on transition-metal oxides: Iron and cobalt phthalocyanine on epitaxial mno and tio x films. *The Journal of Physical Chemistry C*, 119(49):27569–27579, 2015. doi: 10.1021/acs.jpcc.5b09612.

[73] Bradley J Brennan, Alec C Durrell, Matthieu Koepf, Robert H Crabtree, and Gary W Brudvig. Towards multielectron photocatalysis: a porphyrin array for lateral hole transfer and capture on a metal oxide surface. *Physical Chemistry Chemical Physics*, 17(19):12728–12734, 2015. doi: 10.1039/C5CP01683E.

[74] Y Zidon, Yoram Shapira, and Th Dittrich. Illumination induced charge separation at tetraphenyl-porphyrin/metal oxide interfaces. *Journal of Applied Physics*, 102(5), 2007. doi: 10.1063/1.2777200.

[75] A. A. Serga A. V. Chumak, V. I. Vasyuchka and B. Hillebrands. Magnon spintronics. *Nature Physics*, 11:453–461, 2015. doi: 10.1038/nphys3347.

[76] Sergio M. Rezende. Quantum theory of spin waves: Magnons. *Fundamentals of Magnonics*, 2020.

[77] V. V. Kruglyak, S. O. Demokritov, and D. Grundler. Magnonics. *Journal of Physics D: Applied Physics*, 43(26):264001, 2010. doi: 10.1088/0022-3727/43/26/264001.

[78] Baldovi JJ. Rivero-Carracedo G, Rybakov A. Magnon Sensing of NO, NO2 and NH3 Gas Capture on CrSBr Monolayer. *Chemistry*, 2024. doi: 10.1002/chem.202401092.

[79] Alberto M. Ruiz, Gonzalo Rivero-Carracedo, Andrey Rybakov, Sourav Dey, and José J. Baldoví. Towards molecular controlled magnonics. *Nanoscale Adv.*, 2024. doi: 10.1039/D4NA00230J.

[80] J. E. Hirsch. Spin hall effect. *Phys. Rev. Lett.*, 83:1834–1837, Aug 1999. doi: 10.1103/PhysRevLett.83.1834.

[81] K.I. Uchida, S Takahashi, K Harii, J Ieda, W Koshibae, Kazuya Ando, S Maekawa, and E Saitoh. Observation of the spin seebeck effect. *Nature*, 455(7214):778–781, 2008. doi: 10.1038/nature07321.

[82] Zhen Xu, Jing Liu, Shimin Hou, and Yongfeng Wang. Manipulation of molecular spin state on surfaces studied by scanning tunneling microscopy. *Nanomaterials*, 10(12):2393, 2020. doi: 10.3390/nano10122393.

[83] Philip Willke, Tobias Bilgeri, Xue Zhang, Yu Wang, Christoph Wolf, Herve Aubin, Andreas Heinrich, and Taeyoung Choi. Coherent spin control of single molecules on a surface. *ACS nano*, 15(11):17959–17965, 2021. doi: 10.1021/acsnano.1c06394.

[84] Andreas Windischbacher and Peter Puschnig. Computational study on the adsorption of small molecules to surface-supported Ni-porphyrins. *Inorganica Chimica Acta*, 558:121719, 2023. ISSN 0020-1693. doi: 10.1016/j.ica.2023.121719.

[85] Iulia Cojocariu, Silvia Carlotto, Maximilian Sturmeit Henning, Giovanni Zamborlini, Mirko Cinchetti, Albano Cossaro, Alberto Verdini, Luca Floreano, Matteo Jugovac, Peter Puschnig and others. Ferrous to ferric transition in Fe-phthalocyanine driven by NO2 exposure. *Chemistry-A European Journal*, 27(10):3526–3535, 2021. doi: 10.1002/chem.202004932.

[86] de la Torre Bruno, Švec Martin, Redondo Jesus Hapala Prokop, Krejčí Ondřej, Lo Rabindranath, Manna Debashree, Sarmah Amrit, Nachtigallová Dana, and Tuček Jiří et al. Non-covalent control of spin-state in metal-organic complex by

positioning on N-doped graphene. *Nature communications*, 9(1):2831, 2018. doi: 10.1038/s41467-018-05163-y.

[87] Shamik Chakraborty, Guido Fratesi, and Abhilash Ravikumar. Defect controlled spin state transitions in FePc adsorbed CrI3. *Surfaces and Interfaces*, 50:104452, 2024. ISSN 2468-0230. doi: 10.1016/j.surfin.2024.104452.

[88] Antonio Azevedo Rezende, Sergio M. and Roberto L. Rodríguez-Suárez. Introduction to antiferromagnetic magnons. *Journal of Applied Physics*, 126(15), 2019. doi: 10.1063/1.5109132.

[89] O. Gomonay, T. Jungwirth, and J. Sinova. Concepts of antiferromagnetic spintronics (phys. status solidi rrl 4/2017). *physica status solidi (RRL) – Rapid Research Letters*, 11(4):1770319, 2017. doi: 10.1002/pssr.201770319.

[90] V. Baltz, A. Manchon, M. Tsoi, T. Moriyama, T. Ono, and Y. Tserkovnyak. Antiferromagnetic spintronics. *Rev. Mod. Phys.*, 90:015005, Feb 2018. doi: 10.1103/RevModPhys.90.015005.

[91] H. Meer, O. Gomonay, A. Wittmann, and M. Kläui. Antiferromagnetic insulatronics: Spintronics in insulating 3d metal oxides with antiferromagnetic coupling. *Applied Physics Letters*, 122(8):080502, 02 2023. ISSN 0003-6951. doi: 10.1063/5.0135079.

[92] Danrong Xiong, Yuhao Jiang, Kewen Shi, Ao Du, Yuxuan Yao, Zongxia Guo, Daoqian Zhu, Kaihua Cao, Shouzhong Peng, Wenlong Cai, Dapeng Zhu, and Weisheng Zhao. Antiferromagnetic spintronics: An overview and outlook. *Fundamental Research*, 2(4):522–534, 2022. ISSN 2667-3258. doi: 10.1016/j.fmre.2022.03.016.

[93] María D. Manrique-Juárez, Sylvain Rat, Lionel Salmon, Gábor Molnár, Carlos M. Quintero, Liviu Nicu, Helena J. Shepherd, and Azzedine Bousseksou. Switchable molecule-based materials for micro- and nanoscale actuating applications: Achievements and prospects. *Coordination Chemistry Reviews*, 308:395–408, 2016. ISSN 0010-8545. doi: 10.1016/j.ccr.2015.04.005. Perspectives in Coordination Chemistry on the Occasion of the 40th anniversary of the LCC-CNRS, Toulouse, France.

[94] Marco Marino, Elena Molteni, Simona Achilli, Giovanni Onida, and Guido Fratesi. Ab initio electronic, magnetic, and optical properties of Fe-phthalocyanine on Cr2O3(0001). *Molecules*, 29(12), 2024. ISSN 1420-3049. doi: 10.3390/molecules29122889.

[95] Simon Streib, Nicolas Vidal-Silva, Ka Shen, and Gerrit EW Bauer. Magnon-phonon interactions in magnetic insulators. *Physical Review B*, 99(18):184442, 2019. doi: 10.1103/PhysRevB.99.184442.

[96] Bae Youn Jue et al. Exciton-coupled coherent magnons in a 2d semiconductor. *Nature*, 609:282–286, 2022. doi: 10.1038/s41586-022-05024-1.

[97] Thomas L Gilbert. Hohenberg-kohn theorem for nonlocal external potentials. *Physical Review B*, 12(6):2111, 1975. doi: 10.1103/PhysRevB.12.2111.

[98] Walter Kohn and L Sham. Density functional theory. In *Conference Proceedings-Italian Physical Society*, volume 49, pages 561–572. Editrice Compositori, 1996.

[99] Richard M. Martin. *Electronic structure: basic theory and practical methods*. Cambridge university press, 2020.

[100] Erich Runge and Eberhard KU Gross. Density-functional theory for time-dependent systems. *Physical review letters*, 52(12):997, 1984. doi: 10.1103/PhysRevLett.52.997.

[101] Miguel A.L. Marques and Eberhard K.U. Gross. *Time-dependent density functional theory*, volume 55. Annual Reviews, 2004.

[102] Richard M Martin, Lucia Reining, and David M Ceperley. *Interacting electrons*. Cambridge University Press, 2016.

[103] Gianluca Stefanucci and Robert Van Leeuwen. *Nonequilibrium many-body theory of quantum systems: a modern introduction*. Cambridge University Press, 2013.

[104] Lucia Reining. The GW approximation: content, successes and limitations. *Wiley Interdisciplinary Reviews: Computational Molecular Science*, 8(3):e1344, 2018. doi: 10.1002/wcms.1344.

[105] Falco Hüser, Thomas Olsen, and Kristian S Thygesen. Quasiparticle GW calculations for solids, molecules, and two-dimensional materials. *Physical Review B—Condensed Matter and Materials Physics*, 87(23):235132, 2013. doi: 10.1103/PhysRevB.87.235132.

[106] Onida Giovanni, Lucia Reining and Angel Rubio. Electronic excitations: density-functional versus many-body green's-function approaches. *Reviews of modern physics*, 74(2):601, 2002. doi: 10.1103/RevModPhys.74.601.

[107] G. Strinati. Application of the green's functions method to the study of the optical properties of semiconductors. *La Rivista del Nuovo Cimento*, 11(12):1826–9850, 1988. doi: 10.1007/BF02725962.

[108] Alejandro José Uría-Álvarez, Juan José Esteve-Paredes, M.A. García-Blázquez, and Juan José Palacios. Efficient computation of optical excitations in two-dimensional materials with the xatu code. *Computer Physics Communications*, 295:109001, 2024. ISSN 0010-4655. doi: 10.1016/j.cpc.2023.109001.

[109] S Toth and B Lake. Linear spin wave theory for single-q incommensurate magnetic structures. *Journal of Physics: Condensed Matter*, 27(16):166002, 2015. doi: 10.1088/0953-8984/27/16/166002.

[110] Robert M White, Robert M White, and Bradford Bayne. *Quantum theory of magnetism*, volume 1. Springer, 1983.

[111] J.H.P. Colpa. Diagonalization of the quadratic boson hamiltonian. *Physica A: Statistical Mechanics and its Applications*, 93(3):327–353, 1978. ISSN 0378-4371. doi: 10.1016/0378-4371(78)90160-7.

[112] A.I. Liechtenstein, M.I. Katsnelson, V.P. Antropov, and V.A. Gubanov. Local spin density functional approach to the theory of exchange interactions in ferromagnetic metals and alloys. *Journal of Magnetism and Magnetic Materials*, 67(1):65–74, 1987. ISSN 0304-8853. doi: https://doi.org/10.1016/0304-8853(87)90721-9.

[113] Attila Szilva, Yaroslav Kvashnin, Evgeny A Stepanov, Lars Nordström, Olle Eriksson, Alexander I Lichtenstein, and Mikhail I Katsnelson. Quantitative theory of magnetic interactions in solids. *Reviews of Modern Physics*, 95(3):035004, 2023. doi: 10.1103/RevModPhys.95.035004.

[114] Xu He, Nicole Helbig, Matthieu J. Verstraete, and Eric Bousquet. TB2J: A python package for computing magnetic interaction parameters. *Computer Physics Communications*, 264:107938, 2021. ISSN 0010-4655. doi: 10.1016/j.cpc.2021.107938.

[115] Dm M. Korotin and et al. Calculation of exchange constants of the heisenberg model in plane-wave-based methods using the green's function approach. *Physical Review B*, 91, 2015. doi: 10.1103/PhysRevB.91.224405.

[116] I. V. Solovyev. Exchange interactions and magnetic force theorem. *Phys. Rev. B*, 103:104428, Mar 2021. doi: 10.1103/PhysRevB.103.104428.

[117] P. Giannozzi, S. Baroni, N. Bonini, M. Calandra, R. Car, C. Cavazzoni, D. Ceresoli,

G. L. Chiarotti, M. Cococcioni, I. Dabo, A. Dal Corso, S. de Gironcoli, S. Fabris, G. Fratesi, R. Gebauer, U. Gerstmann, C. Gougoussis, A. Kokalj, M. Lazzeri, L. Martin-Samos, N. Marzari, F. Mauri, R. Mazzarello, S. Paolini, A. Pasquarello, L. Paulatto, C. Sbraccia, S. Scandolo, G. Sclauzero, A. P. Seitsonen, A. Smogunov, P. Umari, and R. M. Wentzcovitch. Quantum ESPRESSO: a modular and open-source software project for quantum simulations of materials. *J. Phys.: Condens. Mat.*, 21:395502, 2009. doi: 10.1088/0953-8984/21/39/395502.

[118] P Giannozzi, O Andreussi, T Brumme, O Bunau, M Buongiorno Nardelli, M Calandra, R Car, C Cavazzoni, D Ceresoli, M Cococcioni, N Colonna, I Carnimeo, A Dal Corso, S de Gironcoli, P Delugas, R A DiStasio Jr, A Ferretti, A Floris, G Fratesi, G Fugallo, R Gebauer, U Gerstmann, F Giustino, T Gorni, J Jia, M Kawamura, H-Y Ko, A Kokalj, E Küçükbenli, M Lazzeri, M Marsili, N Marzari, F Mauri, N L Nguyen, H-V Nguyen, A Otero de-la Roza, L Paulatto, S Poncé, D Rocca, R Sabatini, B Santra, M Schlipf, A P Seitsonen, A Smogunov, I Timrov, T Thonhauser, P Umari, N Vast, X Wu, and S Baroni. Advanced capabilities for materials modelling with quantum espresso. *J. Phys.: Condensed Matter*, 29:465901, 2017. doi: 10.1088/1361-648X/aa8f79.

[119] Marco Marino, Elena Molteni, Simona Achilli, and Guido Fratesi. Ab-initio electronic, magnetic, and optical properties of Fe-phthalocyanine on NiO(001). *Inorganica Chimica Acta*, 562:121877, 2024. ISSN 0020-1693. doi: https://doi.org/10.1016/j.ica.2023.121877.

[120] Stefano Baroni, Stefano de Gironcoli, Andrea Dal Corso, and Paolo Giannozzi. Phonons and related crystal properties from density-functional perturbation theory. *Rev. Mod. Phys.*, 73:515–562, Jul 2001. doi: 10.1103/RevModPhys.73.515.

[121] Iurii Timrov, Nicola Marzari, and Matteo Cococcioni. Hubbard parameters from density-functional perturbation theory. *Physical Review B*, 98(8):085127, 2018.

[122] V.R. Cooper. Van der Waals density functional: An appropriate exchange functional. *Phys. Rev. B*, 81:161104, 2010. doi: 10.1103/physrevb.81.161104.

[123] K. Lee, E. D. Murray, L. Kong, B. I. Lundqvist, and D. C. Langreth. Higher-accuracy van der Waals density functional. *Phys. Rev. B*, 82:081101, 2010. doi: 10.1103/PhysRevB.82.081101.

[124] K. F. Garrity, J. W. Bennett, K. M. Rabe, and D. Vanderbilt. Pseudopotentials for high-throughput DFT calculations. *Computational Materials Science*, 81:446–452, 2014. doi: 10.1016/j.commatsci.2013.08.053.

[125] D Sangalli et al. Many-body perturbation theory calculations using the yambo code. *Journal of Physics: Condensed Matter*, 31:325902, 2019. doi: 10.1088/1361-648x/ab15d0.

[126] M. J. van Setten, M. Giantomassi, E. Bousquet, M. Verstraete, D. R. Hamann, X. Gonze, and G.-M. Rignanese. The pseudodojo: Training and grading a 85 element optimized norm-conserving pseudopotential table. *Computer Physics Communications*, 226:39–54, 2018. doi: 10.1016/j.cpc.2018.01.012.

[127] J. P. Perdew, K. Burke, and M. Ernzerhof. Generalized gradient approximation made simple. *Phys. Rev. Lett.*, 77:3865, 1996. doi: 10.1103/PhysRevLett.77.3865.

[128] Carlo Adamo and Vincenzo Barone. Toward reliable density functional methods without adjustable parameters: The pbe0 model. *The Journal of chemical physics*, 110 (13):6158–6170, 1999. doi: 10.1063/1,478522.

[129] Arash A Mostofi, Jonathan R Yates, Giovanni Pizzi, Young-Su Lee, Ivo Souza, David Vanderbilt, and Nicola Marzari. An updated version of wannier90: A tool for obtaining maximally-localised wannier functions. *Computer Physics Communi-*

cations, 185(8):2309–2310, 2014.

[130] Marco Marino. Magnons. `https://github.com/marcomarino123/Magnons.git/`, 2023. [Online].

[131] Marco Marino. BSE. `https://github.com/marcomarino123/BSE.git/`, 2023. [Online].

[132] Conrad Sanderson and Ryan R. Curtin. Armadillo: a template-based c++ library for linear algebra. *J. Open Source Softw.*, 1:26, 2016.

[133] OpenMP Architecture Review Board. OpenMP application program interface version 3.0, May 2008. URL `http://www.openmp.org/mp-documents/spec30.pdf`.

[134] Alessandro Facchin, Daniel Forrer, Mirco Zerbetto, Francesco Cazzadori, Andrea Vittadini, and Christian Durante. Single-site catalysts for the oxygen reduction reaction: Why iron is better than platinum. *ACS Catalysis*, 0(0):14373–14386, 0. doi: 10.1021/acscatal.4c02366.

[135] Alexander B Sorokin. Phthalocyanine metal complexes in catalysis. *Chemical reviews*, 113(10):8152–8191, 2013. doi: 10.1021/cr4000072.

[136] Christian Wäckerlin, Dorota Chylarecka, Armin Kleibert, Kathrin Müller, Cristian Iacovita, Frithjof Nolting, Thomas A Jung, and Nirmalya Ballav. Controlling spins in adsorbed molecules by a chemical switch. *Nature communications*, 1(1):61, 2010. doi: 10.1038/ncomms1057.

[137] Cristina Isvoranu, B Wang, Karina Schulte, Evren Ataman, Jan Knudsen, Jesper N Andersen, ML Bocquet, and Joachim Schnadt. Tuning the spin state of iron phthalocyanine by ligand adsorption. *Journal of Physics: Condensed Matter*, 22(47): 472002, 2010. doi: 10.1088/0953-8984/22/47/472002.

[138] Cristina Isvoranu, Bin Wang, Evren Ataman, Karina Schulte, Jan Knudsen, Jesper N Andersen, Marie-Laure Bocquet, and Joachim Schnadt. Ammonia adsorption on iron phthalocyanine on Au(111): Influence on adsorbate-substrate coupling and molecular spin. *The Journal of chemical physics*, 134(11), 2011. doi: 10.1063/1.3563635.

[139] Giulia Avvisati, Claudia Cardoso, Daniele Varsano, Andrea Ferretti, Pierluigi Gargiani, and Maria Grazia Betti. Ferromagnetic and antiferromagnetic coupling of spin molecular interfaces with high thermal stability. *Nano Letters*, 18(4):2268–2273, 2018. doi: 10.1021/acs.nanolett.7b04836.

[140] Davidson Ernest R. and Weston Thatcher Borden. Symmetry breaking in polyatomic molecules: real and artifactual. *The Journal of Physical Chemistry*, 87:4783–4790, 1983. doi: 0.1007/s00339-008-5005-1.

[141] Dana Nachtigallová, Andrej Antalík, Rabindranath Lo, Robert Sedlák, Debashree Manna, Jiří Tuček, Juri Ugolotti, Libor Veis, Örs Legeza, Jiří Pittner, Radek Zbořil, and Pavel Hobza. An isolated molecule of iron(ii) phthalocyanin exhibits quintet ground-state: A nexus between theory and experiment. *Chemistry – A European Journal*, 24(51):13413–13417, 2018. doi: 10.1002/chem.201803380.

[142] Javier Fernández-Rodríguez, Brian Toby, and Michel van Veenendaal. Mixed configuration ground state in iron(ii) phthalocyanine. *Phys. Rev. B*, 91:214427, Jun 2015. doi: 10.1103/PhysRevB.91.214427.

[143] Marom Noa and Leeor Kronik. Density functional theory of transition metal phthalocyanines, ii: electronic structure of MnPc and FePc—symmetry and symmetry breaking. *Applied Physics A*, 95:165–172, 2009. doi: 10.1007/s00339-008-5005-1.

[144] John P Perdew, Kieron Burke, and Yue Wang. Generalized gradient approximation

for the exchange-correlation hole of a many-electron system. *Physical review B*, 54 (23):16533, 1996. doi: 10.1103/PhysRevB.54.16533.

[145] Barbara Brena, Carla Puglia, Monica de Simone, Marcello Coreno, Kartick Tarafder, Vitaly Feyer, Rudra Banerjee, Emmanuelle Göthelid, Biplab Sanyal, Peter M. Oppeneer, and Olle Eriksson. Valence-band electronic structure of iron phthalocyanine: An experimental and theoretical photoelectron spectroscopy study. *The Journal of Chemical Physics*, 134:074312, 2011. doi: 10.1063/1.3554212.

[146] Iulia Emilia Brumboiu, Soumyajyoti Haldar, Johann Lüder, Olle Eriksson, Heike C. Herper, Barbara Brena, and Biplab Sanyal. Influence of electron correlation on the electronic structure and magnetism of transition-metal phthalocyanines. *Journal of Chemical Theory and Computation*, 12:1772–1785, 2016. doi: 10.1021/acs.jctc.6b00091.

[147] M. D. Kuz'min, A. Savoyant, and R. Hayn. Ligand field parameters and the ground state of Fe(II) phthalocyanine. *The Journal of Chemical Physics*, 138(24): 244308, 06 2013. ISSN 0021-9606. doi: 10.1063/1.4811110.

[148] Philipp Gütlich and Harold A Goodwin. *Spin crossover in transition metal compounds I*, volume 1. Springer Science & Business Media, 2004.

[149] Jian Zhou, Qian Wang, Qiang Sun, Yoshiyuki Kawazoe, and Puru Jena. Strain-induced spin crossover in phthalocyanine-based organometallic sheets. *The Journal of Physical Chemistry Letters*, 3(21):3109–3114, 2012. doi: 10.1021/jz301303t.

[150] W. Neubeck, C. Vettier, F. de Bergevin, F. Yakhou, D. Mannix, L. Ranno, and T. Chatterji. Orbital moment determination of simple transition metal oxides using magnetic x-ray diffraction. *Journal of Physics and Chemistry of Solids*, 62(12):2173–2180, 2001. ISSN 0022-3697. doi: https://doi.org/10.1016/S0022-3697(01)00175-5.

[151] A Schrön, Claudia Rödl, and Friedhelm Bechstedt. Crystalline and magnetic anisotropy of the 3 d-transition metal monoxides MnO, FeO, CoO, and NiO. *Physical Review B—Condensed Matter and Materials Physics*, 86(11):115134, 2012. doi: 10.1103/PhysRevB.86.115134.

[152] Ayato Iyama and Tsuyoshi Kimura. Magnetoelectric hysteresis loops in cr 2 o 3 at room temperature. *Physical Review B—Condensed Matter and Materials Physics*, 87 (18):180408, 2013. doi: 10.1103/PhysRevB.87.180408.

[153] Xiangtian Bu and Yuanchang Li. Optical signature for distinguishing between mott-hubbard, intermediate, and charge-transfer insulators. *Physical Review B*, 106 (24):L241101, 2022. doi: 10.1103/PhysRevB.106.L241101.

[154] Guido Fratesi, Daniele Paoloni, Luca Persichetti, Luca Camilli, Antonio Caporale, Anu Baby, Dean Cvetko, Gregor Kladnik, Alberto Morgante, and Alessandro Ruocco. Spontaneous transmetalation at the ZnPc/Al(100) interface. *Inorganica Chimica Acta*, 559:121790, 2024. ISSN 0020-1693. doi: 10.1016/j.ica.2023.121790.

[155] A Schrön and F Bechstedt. Spin-dependent properties and images of MnO, FeO, CoO, and NiO (001) surfaces. *Physical Review B*, 92(16):165112, 2015. doi: 10.1103/PhysRevB.92.165112.

[156] C. Rödl, F. Fuchs, J. Furthmüller, and F. Bechstedt. Quasiparticle band structures of the antiferromagnetic transition-metal oxides MnO, FeO, CoO, and NiO. *Phys. Rev. B*, 79:235114, 2009. doi: 10.1103/PhysRevB.79.235114.

[157] D. Betto, Y. Y. Peng, S. B. Porter, G. Berti, A. Calloni, G. Ghiringhelli, and N. B. Brookes. Three-dimensional dispersion of spin waves measured in nio by resonant inelastic x-ray scattering. *Phys. Rev. B*, 96:020409, Jul 2017. doi: 10.1103/PhysRevB.96.020409.

[158] Guntram Fischer, Markus Däne, Arthur Ernst, Patrick Bruno, Martin Lüders,

Zdzislawa Szotek, Walter Temmerman, and Wolfram Hergert. Exchange coupling in transition metal monoxides: Electronic structure calculations. *Phys. Rev. B*, 80: 014408, Jul 2009. doi: 10.1103/PhysRevB.80.014408.

[159] R Logemann, A N Rudenko, M I Katsnelson, and A Kirilyuk. Exchange interactions in transition metal oxides: the role of oxygen spin polarization. *Journal of Physics: Condensed Matter*, 29(33):335801, jul 2017. doi: 10.1088/1361-648X/aa7b00.

[160] Daniel Zwillinger and Stephen Kokoska. *CRC standard probability and statistics tables and formulae*. Crc Press, 1999.

[161] Maurice G Kendall and Alan Stuart. The advanced theory of statistics. vol. 3. *Biometrics*, 25(2):435, 1969.

[162] Mildred S Dresselhaus, Gene Dresselhaus, and Ado Jorio. *Group theory: application to the physics of condensed matter*. Springer Science & Business Media, 2007.

[163] Arthur P Cracknell. Magnetic groups. *Contemporary Physics*, 8(5):459–473, 1967. doi: 10.1088/0034-4885/32/2/305.

[164] C.J. Bradley and B.L. Davies. Magnetic groups and their corepresentations. *Reviews of Modern Physics*, 40(2):359, 1968.

[165] Luis Elcoro, Benjamin J Wieder, Zhida Song, Yuanfeng Xu, Barry Bradlyn, and B Andrei Bernevig. Magnetic topological quantum chemistry. *Nature communications*, 12(1):5965, 2021. doi: 10.1038/s41467-021-26241-8.

[166] Yuanfeng Xu, Luis Elcoro, Zhi-Da Song, Benjamin J Wieder, MG Vergniory, Nicolas Regnault, Yulin Chen, Claudia Felser, and B Andrei Bernevig. High-throughput calculations of magnetic topological materials. *Nature*, 586(7831):702–707, 2020. doi: 10.1038/s41586-020-2837-0.

[167] Alberto Corticelli, Roderich Moessner, and Paul A. McClarty. Identifying and constructing complex magnon band topology. *Phys. Rev. Lett.*, 130:206702, May 2023. doi: 10.1103/PhysRevLett.130.206702.

[168] Sergio M. Rezende, Antonio Azevedo, and Roberto L. Rodríguez-Suárez. Introduction to antiferromagnetic magnons. *Journal of Applied Physics*, 126(15):151101, 10 2019. ISSN 0021-8979. doi: 10.1063/1.5109132.

[169] Alexandre C Dias, Julian FRV Silveira, and Fanyao Qu. Wantibexos: A wannier based tight binding code for electronic band structure, excitonic and optoelectronic properties of solids. *Computer Physics Communications*, 285:108636, 2023. doi: 10.1016/j.cpc.2022.108636.

[170] Konrad Merkel and Frank Ortmann. Linear scaling approach for optical excitations using maximally localized wannier functions. *Journal of Physics: Materials*, 7 (1):015001, 2023. doi: 10.1088/2515-7639/ad06cd.

[171] Nicola Marzari and David Vanderbilt. Maximally localized generalized wannier functions for composite energy bands. *Phys. Rev. B*, 56:12847–12865, Nov 1997. doi: 10.1103/PhysRevB.56.12847.

[172] Xiaofan Yang, Xiaoming Liu, Shuo Yu, Lu Gan, Jun Zhou, and Yonghu Zeng. Permittivity of undoped silicon in the millimeter wave range. *Electronics*, 8(8):886, 2019. doi: 10.3390/electronics8080886.

[173] H.W. Icenogle, Ben C. Platt, and William L. Wolfe. Refractive indexes and temperature coefficients of germanium and silicon. *Applied optics*, 15(10):2348–2351, 1976. doi: 10.1364/AO.15.002348.

[174] Stefano Baroni and Raffaele Resta. Ab initio calculation of the macroscopic dielectric constant in silicon. *Physical Review B*, 33(10):7017, 1986. doi: 10.1103/PhysRevB.33.7017.

[175] K.V. Rao and A. Smakula. Dielectric properties of cobalt oxide, nickel oxide, and their mixed crystals. *Journal of Applied Physics*, 36(6):2031–2038, 1965. doi: 10.1063/1.1714397.

List of Publications

As of Sept. 20^{th}, 2024

Refereed publications

- M. Marino, E. Molteni, S. Achilli, G. Onida and G. Fratesi, Ab-initio electronic, magnetic, and optical properties of Fe- phthalocyanine on Cr2O3(0001), Molecules, 29, 2889, 2024
- M. Marino, E. Molteni, S. Achilli and G. Fratesi, Ab-initio electronic, magnetic, and optical properties of Fe- phthalocyanine on NiO(001), Inorganica Chimica Acta, 562, 2024
- L. Gnoli, M. Benini, C. Del Conte, A. Riminucci, R. Rakshit, M. Singh, S. Sanna, R. Yadav, K. Lin, A. Mezzi, S. Achilli, E. Molteni, M. Marino, G. Fratesi, V. A. Dediu and Ilaria Bergenti, Enhancement of Magnetic Stability in Antiferromagnetic CoO Films by Adsorption of Organic Molecules, Applied Electronic Materials, 6, 3138-3146, 2024.
- Fratesi, S. Achilli, G. Onida, F. Orlando, M. Marino, E. Molteni, G. Onida, Tuning electronic and magnetic properties of ultrathin and bulk magnetic oxides by adsorption of organic molecules, IL NUOVO CIMENTO C,104, 109.1-109.4, 2023

Publications under review

- M. Capra, M. Marino, A. Picone, A. Ferretti, A. Giampietri, F. Ciccacci, S. Fiori, D. Dagur, F. Motti, G. Vinai, G. Panaccione, E. Molteni, S. Achilli, G. Fratesi, A. Brambilla, Long-range Magnetic Ordering of FePc Molecules Driven by Interfacial Coupling with Antiferromagnetic Cr2O3, Advanced Physics Research, 2024

Publications in preparation

- M. Marino et al., Chemical Tuning of Magnons in NiO(001) by Fe-phthalocyanine Adsorption
- M. Marino et al., Ab-initio electronic, magnetic, and optical properties of Fe-phthalocyanine on CoO(001)

Acknowledgments

Diverse persone hanno permesso questo lavoro, con la loro presenza, il loro ascolto ed il loro sostegno. Penso che la vita sia ben più capace di noi nel trovare le parole adatte a raccontarci. Per cui mi limito a ringraziarle, con riconoscente gratitudine. Ringrazio i miei genitori, i miei nonni ed i miei zii che mi hanno accompagnato e sostenuto nel mio percorso di vita e accademico. Ringrazio i miei fratelli Francesca, Chiara e Andrea, presenza costante e gioiosa della mia vita. Ringrazio Tommaso Braguglia, Francesco Marabotti, Manfredi Comella e Giovanni Tobia, miei cari amici. Ringrazio i miei compagni di percorso per i momenti passati insieme, Gianluca Martini, Filippo Profumo, Hatice Holuigue, Giacomo Nadalini, Davide Decca, Stefano Radice, Silvia Bressan e Lorenzo Dal Fabbro. Ringrazio Andrey Rybakov, che ha dato alla mia ricerca una svolta inaspettata. Ringrazio Gonzalo Rivero-Carracedo, Alberto M. Ruiz, Dorye Esteras, Diego López-Alcalá e Sourav Dey. Ringrazio i miei relatori per la loro pazienza, per il loro aiuto e per i loro consigli, Guido Fratesi e Simona Achilli. Ringrazio i diversi collaboratori, tra cui in particolar modo Elena Molteni e Michele Capra. Ringrazio i miei cari amici toscani Luca Garinetti e Lorenzo Manfredini e la mia cara amica biellese Francesca Gobbo. Ringrazio Giuseppe, che ha visto molti venire e molti andare, ma è sempre rimasto per accoglierli e per salutarli. Ringrazio i due referees Peter Puschnig e Matteo Cococcioni senza i quali questo lavoro non sarebbe nella forma attuale. E ringrazio le persone che ho incontrato in questi tre anni e con cui ho condiviso del tempo, che hanno reso questo lavoro anche più piacevole.